Research Article

Design of a High-Throughput Human Neural Crest Cell Migration Assay to Indicate Potential Developmental Toxicants

Johanna Nyffeler [1,2], Christiaan Karreman [1], Heidrun Leisner [1], Yong Jun Kim [4,5], Gabsang Lee [4,5], Tanja Waldmann [1] and Marcel Leist [1,2,3]

[1]In vitro Toxicology and Biomedicine, Dept inaugurated by the Doerenkamp-Zbinden Foundation at the University of Konstanz, Konstanz, Germany; [2]Research Training Group RTG1331, University of Konstanz, Konstanz, Germany; [3]Konstanz Research School Chemical Biology (KoRS-CB), University of Konstanz, Konstanz, Germany; [4]Institute for Cell Engineering, Johns Hopkins University School of Medicine, Baltimore, MD, USA; [5]Department of Neurology, Johns Hopkins University School of Medicine, Baltimore, MD, USA

Summary

Migration of neural crest cells (NCCs) is one of the pivotal processes of human fetal development. Malformations arise if NCC migration and differentiation are impaired genetically or by toxicants. In the currently available test systems for migration inhibition of NCC (MINC), the manual generation of a cell-free space results in extreme operator dependencies, and limits throughput. Here a new test format was established. The assay avoids scratching by plating cells around a commercially available circular stopper. Removal of the stopper barrier after cell attachment initiates migration. This microwell-based circular migration zone NCC function assay (cMINC) was further optimized for toxicological testing of human pluripotent stem cell (hPSC)-derived NCCs. The challenge of obtaining data on viability and migration by automated image processing was addressed by developing a freeware. Data on cell proliferation were obtained by labelling replicating cells, and by careful assessment of cell viability for each experimental sample. The role of cell proliferation as an experimental confounder was tested experimentally by performing the cMINC in the presence of the proliferation-inhibiting drug cytosine arabinoside (AraC), and by a careful evaluation of mitotic events over time. Data from these studies led to an adaptation of the test protocol, so that toxicant exposure was limited to 24 h. Under these conditions, a prediction model was developed that allows classification of toxicants as either inactive, leading to unspecific cytotoxicity, or specifically inhibiting NC migration at non-cytotoxic concentrations.

Keywords: cell tracking, cell proliferation, high content imaging, developmental toxicity, human stem cells

1 Introduction

The design and optimization of human-relevant test systems for developmental toxicity is an important challenge for modern toxicology research. Animal-based tests lack the throughput required to evaluate the large number (Rovida and Hartung, 2009; Crofton et al., 2012; Smirnova et al., 2014; Bennett et al., 2016) of untested substances, and they are animal- and resource-intensive. Moreover, they require that results are extrapolated from the test animal to humans, a particularly difficult task where the development of the immune and nervous systems are concerned. Thus, it has been proposed to focus on tests based mainly on human cells. A recent study based on 10,000 chemical profiles modelled in the Tox21 effort demonstrated the advantage of human cells over animal cells in predicting human toxicity hazard (Huang et al., 2016). The increased use

Abbreviations

AraC, cytosine arabinoside; BDNF, brain-derived neurotrophic factor; BMC, benchmark concentration; cMINC, circular MINC; DMSO, dimethyl sulfoxide; DNT, developmental neurotoxicity; EC, effective concentration; EdU, 5-ethynyl-2'-deoxyuridine; EGF, epidermal growth factor; FBS, fetal bovine serum; FGF, fibroblast growth factor; GUI, graphical user interface; hESC, human embryonic stem cell; HNK-1, human natural killer-1 antigen; iPSC, induced pluripotent stem cell; MINC, migration of neural crest cell; NCC, neural crest cell; NOAEL, no observed adverse effect level; PBS, phosphate buffered saline; PCB, polychlorinated biphenyl; PM, prediction model; p75, low affinity nerve growth factor receptor; ROI, region of interest

Received May 3, 2016;
Accepted July 25, 2016;
Epub July 27, 2016;
https://doi.org/10.14573/altex.1605031

of human cells has become possible due to stem cell technology that allows generation of specific cell types.

Testing of chemicals for developmental toxicity has a high priority, as an increase in the global incidence of developmental disorders was registered in the last two decades. In 2006-2010, the prevalence rate of congenital anomalies in Europe reached 2.4%, with one out of ten specifically related to defects of the nervous system (Dolk et al., 2010). The causes of developmental disorders are extremely heterogeneous. The anomalies can be directly caused by genetic alterations in the embryo, or they can be triggered by chemicals affecting embryonic development. Moreover, they may have an indirect origin associated with maternal exposure to external factors, such as infections, trauma or drugs. A better understanding of the developmental processes and how toxicants affect them is important to identify the causes and to develop strategies to avoid them (Barouki et al., 2012; Grandjean and Landrigan, 2014). This applies to a particularly high degree to the field of developmental neurotoxicity (DNT) (Bal-Price et al., 2012; Crofton et al., 2012).

Modern *in vitro* DNT assays are designed to model a specific biological key event (Leist et al., 2010; Crofton et al., 2011) at defined developmental stages (Stummann et al., 2009; van Dartel et al., 2009; Zimmer et al., 2011; van Thriel et al., 2012). For instance, assays have been developed that assess changes in early neural differentiation (Balmer et al., 2012; Pennings et al., 2012; Theunissen et al., 2012, 2013; Krug et al., 2013b; Balmer et al., 2014; Waldmann et al., 2014; Rempel et al., 2015; Shinde et al., 2015), neurite outgrowth (Stiegler et al., 2011; Krug et al., 2013a), synaptogenesis (Harrill et al., 2011), gliogenesis (Fritsche et al., 2005) or myelination (Zurich et al., 2000, 2002).

A subset of biological key events relates to the specification, migration and differentiation of neural crest cells (NCCs). These specialized cells arise at the time of neurulation and migrate to their target sites in the body, where they give rise to very different cell types such as sensory neurons, glia, melanocytes, adrenal medulla and cranial cartilage/bones. When the finely regulated processes of NCC development and migration are altered, dramatic pathological consequences, called neurocristopathies, can be the result. For example, failure of the NCCs to colonize the gut leads to incomplete innervation of the gastrointestinal tract, as the enteric neurons and glia are derived from the neural crest. This results in Hirschsprung's disease, which affects 1 in 5,000 newborns (Farlie et al., 2004). Another disorder related to the function of NCCs is Treacher-Collins syndrome with a frequency of 1 in 50,000 newborns (Trainor, 2010). Patients have malformed mandibles, ears and teeth as well as cleft palate and eye problems. The etiology of this disease is linked to a diminished number of NCCs migrating to the cranial structures (Trainor, 2010). Other pathologies involving the NC comprise spina bifida, cleft palate and CHARGE syndrome.

Besides genetic causes, neurocristopathies might be caused by chemicals, and several substances are known to interfere with NCC migration. They comprise the anti-epileptic drug valproic acid (found to interfere with NCC migration out of chick neural tube explants, Fuller et al., 2002) and the triazole fungicides (disturbing NC migration in rat embryos, Menegola et al., 2005). However, only few assays that test NCC function have been developed. Some of these tests use *ex vivo* neural tube explants (Fuller et al., 2002; Bergeron et al., 2013; Usami et al., 2014, 2015), but this only allows low throughput testing and the data-analysis is very time-consuming. Furthermore, the use of animal cells might not be relevant for human toxicity, as there are tremendous species differences in the timing of epithelial-to-mesenchymal transition, delamination and migration of NCCs as well as the closure of the neural tube (Theveneau and Mayor, 2012). Moreover, different species express different cell adhesion molecules during NCC development (McKeown et al., 2013). For example, chicken NCCs express cadherin 6B and later cadherin 7 before and after delamination, respectively, whereas in mouse cadherin 6 is expressed in both situations (Pla et al., 2001).

To overcome the above-mentioned limitations, we established an NCC migration assay (MINC assay) using human NCCs differentiated from embryonic stem cells (Zimmer et al., 2012). In this assay, NCC migration is measured as the number of cells repopulating a cell-free area produced by scratching with a pipette-tip. Several known developmental toxicants were positive in the original MINC assay. A screen of recently marketed drugs (Zimmer et al., 2014) and a further exploration of environmental toxicants (Dreser et al., 2015) identified additional NCC toxicants, such as polychlorinated biphenyls and interferon-beta.

Although a semi-automatic image quantification tool already has been established (Dreser et al., 2015), the throughput of the scratch assay is limited by manual image acquisition. Moreover, the assay is highly dependent on the experimenter's skills to achieve reproducible scratch properties. Therefore, we have developed a new assay format to overcome these limitations. Instead of a linear scratch, a circular cell-free area is produced using silicon stoppers of defined size. Image acquisition and analysis are performed in an automated high-throughput manner. This new circular MINC (cMINC) assay was assessed for potential confounding factors that could affect its robustness. This required benchmarking against other readouts related to migration, as well as a careful evaluation of the role of cell proliferation and cell death during the assay time period. A prediction model for functional NCC toxicants was developed.

2 Materials and methods

NCC differentiation

Various pluripotent stem cell lines were used. These included a variant of the H9 line (WA09; WiCell, Wisconsin) with green fluorescent protein (GFP) expression under the control of the Dll1 promotor (H9-Dll1; provided by M. Tomishima, Memorial Sloan Kettering Cancer Centre, New York, NY, USA) as described earlier (Zimmer et al., 2012), the induced pluripotent cell (iPSC) line iPS(IMR90)_clone #4 (Yu et al., 2007) (WiCell, Wisconsin) and iPSC generated from the human fibroblast line GM02036 (Coriell Institute, Camden, New Jersey). Import of human embryonic stem cells (hESC) and all experiments utiliz-

ing them were carried out according to German legislation and under the license of the Robert-Koch Institute (license number 1710-79-1-4-27).

For maintenance culture, H9 cells were maintained on inactivated murine embryonic fibroblasts in DMEM/F12 medium supplemented with 20% serum replacement, 4-(2-hydroxyethyl)-1-piperazineethanesulfonic acid (HEPES), L-glutamine, non-essential amino acids, β-mercaptoethanol (all purchased from Gibco) and fibroblast growth factor 2 (FGF2) (Invitrogen). For the experiments concerned with test establishment, differentiation to NCCs was performed exactly as described earlier (Lee et al., 2010; Zimmer et al., 2012). Briefly, hESC were seeded on inactivated MS-5 stromal cells and differentiated to rosettes using noggin, sonic hedgehog (superSHH), fibroblast growth factor 8 (FGF8), brain-derived neurotrophic factor (BDNF) (all purchased from R&D) and ascorbic acid (Sigma-Aldrich). After 17 to 21 days, the formed rosette structures were picked manually and plated on poly-L-ornithin/fibronectin/laminin coated plates. Upon differentiation with ascorbic acid, BDNF, SHH and FGF8 for another seven days, cells were live-stained for human natural killer-1 (HNK-1, monoclonal anti-human CD57/HNK-1 antibody, Sigma-Aldrich) and FACS-sorted for positive expression of HNK-1 and negative expression of Dll1 using a BD FACSAria IIIu (BD Biosciences). The sorted cells were expanded in N2-S medium, consisting of DMEM/F12 (Gibco) and supplemented with 100 µg/ml apotransferrin, 25 µg/ml insulin, 8.6 mM glucose, 100 µM putrescine, 30 nM selenite, 20 nM progesterone (all purchased from Sigma-Aldrich), 1x GlutaMax and 1% penicillin/streptomycin (both from Gibco), 20 ng/ml epidermal growth factor (EGF) and 20 ng/ml FGF2 (both from R&D). Medium was changed every other day, and cells were passaged every 5-7 days by detachment with HyClone HyQTase (GE Healthcare Life Sciences). After 27-30 days, cells were cryopreserved at $4*10^6$ cells/ml in 90% fetal bovine serum (FBS) (PAA Laboratories GmbH) and 10% dimethyl sulfoxide (DMSO) (Millipore) until further use (Fig. S1A at https://doi.org/10.14573/altex.1605031s). For all migration experiments, freshly thawed NCCs were used and cultured in N2-S medium

Tab. 1: List of chemicals tested in the cMINC assay

Compound	Tested concentrations	LOAEL migration 24 h	Stock concentration (solvent)	CAS #	Catalog #	Provider
Colchicine	1.25 - 20 nM	10 nM	2mM (H_2O)	64-86-8	C9754	Sigma
Taxol	0.3125 - 40 nM	10 nM	10 mM (DMSO)	33069-62-4	1097	Tocris
CytoD	12.5 - 400 nM	200 nM	5 mM (DMSO)	22144-77-0	C8273	Sigma
FBS	0.625 - 4%	2%	–	–	A15-101	PAA
As_2O_3	0.5 - 2 µM	1 µM	100mM (0.1% $NaHCO_3$ in H_2O)	1327-53-3	11099	Sigma
$CdCl_2$	0.1 - 2 µM	0.5 µM	100mM (H_2O)	10108-64-2	655198	Sigma
LiCl	1.25 - 20 mM	10 mM	1 M (H_2O)	7447-41-8	L9650	Sigma
Acrylamide	0.078 - 5 mM	2.5 mM	3.5 M (H_2O)	79-06-1	A3553	Sigma
PCB180	1 - 20 µM	5 µM	20 mM (DMSO)	35065-29-3	35495	Sigma
Retinoic acid	0.156 - 20 µM	5 µM	100mM (DMSO)	302-79-4	R2625	Sigma
Aphidicolin	10 - 1000 ng/ml	1000 ng/ml	1 mg/ml (DMSO)	38966-21-1	A4487	Sigma
AraC	0.001 - 1 µM	1 µM	100 mM (H_2O)	69-74-9	C6645	Sigma
MG-132	12.5 - 400 nM	200 nM	10 mM (DMSO)	133407-82-6	S2619	Selleckchem
Staurosporin	2.5 - 40 nM	40 nM	5mM (DMSO)	62996-74-1	19-123	Millipore
Triton X-100	2.6 - 171 µM	43 µM	1.71 M (pure)	9002-93-1	93443	Sigma
$AgNO_3$	3.125 - 100 µM	50 µM	1 M (H_2O)	7761-88-8	7908.1	Roth
L-Homocysteine thiolactone	0.156 - 5 mM	2.5 mM	500 mM (H_2O)	31828-68-9	H6503	Sigma
NaCl	20 mM	–	1 M (H_2O)	7647-14-5	3957.1	Roth
DMSO	1%	–	–	67-68-5	1096780100	Millipore
EdU	10 µM	–	10 mM (H2O)	61135-33-9	part of kit	PanaTecs

Abbreviations: AraC, cytosine arabinoside hydrochloride; CytoD, cytochalasin D; EdU, 5-ethynyl-2'-deoxyuridine; LOAEL, lowest observed adverse effect level

supplemented with 20 ng/ml EGF and 20 ng/ml FGF2. Exact procedures for the maintenance, differentiation and use of iPSC are detailed in the supplementary file at https://doi.org/10.14573/altex.1605031s.

NCC migration setup

For all experiments, 96-well plates (Corning) were coated with 10 µg/ml poly-L-ornithine in 100 µl phosphate buffered saline (PBS) (PAA Laboratories GmbH) overnight in an incubator, washed three times with 120 µl PBS and further coated with 1 µg/ml fibronectin and 1 µg/ml laminin (both from Sigma-Aldrich) in 100 µl PBS. Plates were stored in the incubator until they were used, but at least overnight and not for more than three weeks.

Before seeding, the fibronectin-laminin solution was aspirated and the plates were dried for 15 min under sterile conditions. Silicon stoppers (Platypus Technologies, Madison, WI, US) of 2.0 mm diameter were inserted into the wells to create a circular cell-free area. Then, freshly thawed NCCs were seeded at a density of 30,000 cells per well (95,000 cells/cm^2) in 100 µl medium. One day after seeding, migration into the cell-free area was initiated by manual removal of the stoppers and the medium was refreshed. For 48 h treatments, test chemicals were applied directly in fresh medium and then left for 48 h without further manipulation. For 24 h treatments, the compounds were added as 5x concentrate after additional 24 h of incubation, and overall migration was measured 24 h after addition of toxicants (i.e., 48 h after the medium change). Toxicants were diluted in medium and the final DMSO concentration did not exceed 0.1%. A list of the test chemicals and the concentrations used is given in Table 1.

Immunocytochemical characterization

For immunocytochemical staining, cells were seeded on plastic or glass, either evenly distributed at usual cell density (p75, GFAP, Pax6 staining) or as drops (20,000 cells per 10 µl drop) to observe migrating cells at the border (Nestin/F-actin co-staining). After one day in culture, cells were fixed with 4% formaldehyde, 2% sucrose in PBS or with ice-cold methanol. For intracellular epitope staining, cells were permeabilized for 15 min with 0.1% Triton and blocked with 10% FBS in PBS for 1 h before primary antibodies were applied in 4% FBS in PBS overnight. The next day, cells were washed with 0.05% Tween in PBS and secondary antibodies were applied (1:1000) for 1 h. Cell nuclei were counterstained with 1 µg/ml H-33342 for 10 min. Images were acquired using an Axio Observer.Z1 microscope (Zeiss, Oberkochen, Germany) equipped with an Axiocam MRm camera. The list of antibodies used is given at https://doi.org/10.14573/altex.1605031s.

For flow cytometric characterization, 120,000 cells were live stained for HNK-1 and p75. Cells were detached, counted and washed once in DMEM containing 10% FBS and subsequently washed in 2% of this mixture in PBS (washing buffer). Primary antibodies were applied for 30 min on ice, followed by two washing steps and incubation with appropriate secondary antibodies for 25 min on ice. After two more washes, cells were analyzed using a BD Accuri C6 flow cytometer (BD Biosciences). In order to set the threshold for HNK-1 positivity, a set of cells was stained only with the secondary antibody. The threshold for positivity was based on the fluorescence intensity distribution of this population, so that 98.6% of this control population were defined as negative, and cells with a higher intensity than this threshold were defined as positive.

Image-based measurement of cell migration and viability

For image acquisition, cells were stained 47.5 h after initiation of migration with 1µg/ml H-33342 and 533 nM calcein-AM (both from Sigma-Aldrich) and imaged 30 min later on a high content imaging microscope (Cellomics ArrayScanVTI, Thermo Fischer) equipped with a Hamamatsu ORCA-ER camera of 1024 x 1024 pixel resolution run at 2 x 2 binning mode. To obtain data on NCC viability, four fields outside the migration area were imaged with a 10x lens (approximately 500 cells/field). To obtain data on cell migration, the center of the well was imaged in four tiles with the 5x lens. The four images were joined to obtain one micrograph covering an area of 2590 x 2590 µm.

Viability was defined as the number of H-33342 and calcein double-positive cells as determined by an automated algorithm described earlier (Stiegler et al., 2011; Krug et al., 2013a).

For quantification of migration, a software tool (freely accessible at http://invitrotox.uni-konstanz.de/) was developed to estimate the most likely position of the previously cell-free area (covered by the silicon stopper), to set thresholds for color intensity for both dyes, and to count the number of H-33342 and calcein double-positive cells in the region of interest (ROI). If treatment was for 48 h, the radius of the circular ROI was set at 1.0 mm. For 24 h treatments, the radius of the ROI was reduced to 0.7-0.9 mm to account for the fact that cells could migrate into the cell-free area for 24 h before the treatment was started. The radius of the reduced ROI was chosen in a way that at least 150 but not more than 300 cells were in the ROI in the untreated condition. A JPEG image of the final picture was generated to visually control the obtained result. The chosen settings were then transferred to all wells. Finally, the software counted the number of viable cells in the ROI for all wells of the plate and a data table was generated with the results. If not mentioned otherwise, viability and migration were normalized to the untreated control.

qPCR

Cells were seeded in 6-well plates at the same cell density as in the migration assay. Medium was exchanged after one day and cells were harvested after two further days and lysed in 1 ml PeqGOLD Trifast™ (PEQlab, Erlangen, Germany). Total RNA was isolated by phenol-chloroform extraction. Briefly, 200 µl chloroform was added, samples were vortexed and incubated for 3 min at room temperature. Then, samples were centrifuged at 4°C for 14 min at 20,000 g. The upper aqueous phase was then transferred to a new vial and mixed with 500 µl isopropanol. After 10 min incubation at room temperature, samples were centrifuged at 4°C for 10 min at 20,000 g. The supernatant was removed and washed twice by carefully adding 1 ml of 75% ice-cold ethanol to the pellet followed by 5 min centrifugation at 10,000 g at 4°C. The pellet was dried for 30 min and 40 µl RNase-free water was added to the samples.

Reverse transcription was performed using 1 µg of RNA and the iScript™ Reverse Transcription Supermix (Bio-Rad, Muenchen, Germany) according to the manufacturer's instructions. Reactions were performed in a volume of 20 µl, and 80 µl of RNase-free water was added afterwards.

Quantitative real-time PCR was carried out using 1 µl of the cDNA solution (with a concentration in the range of 0.1-1 µg/ml), 5 µl SsoFast™ EvaGreen® Supermix (Bio-Rad), 200 µM of each forward and reverse primer (sequences are given at https://doi.org/10.14573/altex.1605031s) in a total volume of 10 µl. Amplification was carried out in 96-well plates on a CFX96™ Real-Time PCR Detection System (Bio-Rad). Samples were heated for 2 min to 98°C, followed by 40 cycles of 2 s at 98°C and 5 s at 60°C. A melt curve from 75°C to 95°C in 0.5°C steps was obtained to measure the presence of primer dimers or other side products. The cycle threshold (Ct) values were determined using the Bio-Rad CFX Manager™ Software v2.0 (Bio-Rad). Results were analyzed using the ΔCt method (Livak and Schmittgen, 2001), i.e., Ct values of the genes of interest were compared to Ct values of the reference gene GAPDH.

Proliferation experiments

To measure proliferation, cells were treated as described in the section "NCC migration setup" with the exception that 10 µM 5-ethynyl-2'-deoxyuridine (EdU), a thymidine analogue, was present during the treatment period. Proliferating cells incorporate EdU, which can later be detected using a click reaction. After imaging, cells were fixed with 4% formaldehyde and 2% sucrose (both from Sigma-Aldrich) in PBS for 20 min. The click reaction to detect EdU was performed according to the manufacturer's protocol (EdU-Click 555, PanaTecs, Heilbronn, Germany) without the permeabilization step and with washing performed with PBS only. Images were acquired using a high content imaging microscope (Cell Insight Personal Imager, Thermo Fischer) equipped with a QUANTIX camera of 1024 x 1024 resolution run at 2 x 2 binning. Proliferation was defined as the percentage of EdU positive nuclei among all H-33342 positive nuclei. As a positive control, cells were treated with 10 µM EdU and 1 µM cytosine arabinoside (AraC), a proliferation inhibitor. Migration was normalized to cells treated with EdU only for an overview of the correlation of EdU incorporation and migration inhibition.

To measure migration under proliferation inhibition, cells were treated as described in the section "NCC migration setup", with the exception that 1 µM AraC was present during the treatment period. Migration was normalized to cells treated with AraC only.

Data handling and statistics

Values are expressed as means ± SD. If not indicated otherwise, experiments were performed at least three times (i.e., using three different cell preparations), with at least three technical replicates per condition. Statistical comparisons of selected experimental conditions vs controls (48 h cMINC assay) were done using an unpaired Student's t-test. Values of $p < 0.05$ were considered statistically significant.

Concentration-response curves from averaged data (n = 3 experiments) were fitted using R (R Core Team, 2015) and the package "drc" (Ritz and Streibig, 2005) to a log-logistic function with four parameters, where the upper asymptote was set to 100%, and appropriate constraints were used for the other parameters. The data points within a curve were weighted with 1/SD; EC90 and EC75 values of the fitted curves were estimated. If the estimated EC was above the highest tested concentration, this concentration was used for further calculations and the greater-than-sign was used. Additionally, "migration at the EC90 of viability" was estimated. If the EC90 was above the highest tested concentration, the extent of migration at the highest tested concentration was used and the smaller-than-sign was used.

3 Results and discussion

3.1 Characterization of the test system

Human NCCs were differentiated from pluripotent stem cells, based on an established protocol (Zimmer et al., 2012) (Fig. S1A, https://doi.org/10.14573/altex.1605031s). For most experiments, the human embryonic stem cell (hESC) line H9 was used. Alternatively, NCCs were generated from human iPSC lines (Fig. S2, https://doi.org/10.14573/altex.1605031s). The protocol ended with an expansion phase of the NCC obtained by FACS sorting. During this time NCC characteristics were well retained as, e.g., measured by the expression of the NCC marker HNK-1 (Fig. S1B). This allowed the generation of large batches of cells that could be frozen and thawed as required for toxicity testing or further characterization of the cells under test conditions. Staining of the cryopreserved cells after thawing showed that ~95% of the cells were positive for at least one NCC marker (Fig. S1C). Immunostaining of cells plated for 24 h revealed that > 99% were positive for the stem cell microfilament protein nestin (not shown), and that nearly all cells expressed the low affinity nerve growth factor receptor p75 (Fig. 1A). Further characterization showed that the NCC neither expressed the astrocyte marker GFAP nor the central nervous system precursor cell marker Pax6 (Fig. S1D). Co-staining for nestin and F-actin microfilaments revealed the mesenchymal-like cell morphology that is typical for NCCs and that clearly differentiates them from other related cell types (Fig. 1A).

Contact of cells to one another and to the extracellular matrix are important biological features in the context of NCC migration and its control. A major group of proteins responsible for matrix contacts are the integrins, while cadherins are key proteins determining cell-cell contact (Fig. 1B). The two groups of proteins are coded by a large family of genes, and the relative expression pattern of the respective family members is cell-type specific. Thus, the expression pattern of several integrins and cadherins was assessed by qPCR.

A broad range of integrin subunits was expressed by the NCCs, and the expression pattern confirmed our earlier data obtained by microarray analysis (Zimmer et al., 2012). Of the β subunits, the highest mRNA-levels were of β1, but β3, β5 and β8 were also highly expressed. Of the α subunits, α1, α4, α5, α8, α11 and αV were highly expressed.

Of the tested integrins, only α6 and β2 were not detected. The subunit coded by β2 (CD18) is a typical leukocyte marker (e.g., also on microglia), and also the absence of α6 in NCCs is consistent with other findings, e.g., in the chicken α6 expression is downregulated at the onset of NCC migration and re-expressed upon neuronal differentiation (Bronner-Fraser et al., 1992; Testaz et al., 1999). The expression pattern quantified here indicates that the integrins could form heterodimers for several substrates, i.e., α1β1 and α11β1 for collagen substrates, α5β1, α8β1, αVβ3, αVβ5, αVβ8 for attachment to fibronectin and vitronectin, and also to some extent α3 and α7-containing dimers to bind laminin (Barczyk et al., 2010). In agreement with these results, the generated NCCs attached well to fibronectin, vitronectin and collagen and to some extent to laminin (data not shown). For the standard assay setup, a coating of poly-ornithine/fibronectin/laminin was used.

To the best of our knowledge, there is no information on integrin expression during human NCC development. However, integrin α4, which was highly expressed according to the qPCR data, has been reported to be expressed at high levels on NCC of several animal species, and it has even been used as a specific NCC marker in mouse development (Kil et al., 1998; Testaz and Duband, 2001). Reports from different animal models also often described α5, αV, β1 and β3 on NCCs (Kil et al., 1998; Testaz et al., 1999; Haack and Hynes, 2001). Several studies in a variety of cell types have linked α4 and α5 to the regulation of cell migration (Mould et al., 1994; Beauvais et al., 1995; Wu et al., 1995); in particular, α4β1 is a typical integrin of highly migratory cell types (Sheppard et al., 1994; Haack and Hynes, 2001).

The more than 1000-fold expression difference between epithelial (E-cadherin, CDH1, low) and neuronal cadherin (N-cadherin, CDH2, high) indicated that the NCCs had undergone epithelial-to-mesenchymal transition (Nieto, 2011) and thus have a high migratory capacity. Other cadherins that showed high expression levels were CDH7, CDH10, CDH11 and CDH20 (Fig. 1B). The knowledge on cadherin expression by human NCC is extremely limited; moreover, pronounced species differences have been observed for this protein family (reviewed in Taneyhill, 2008; Strobl-Mazzulla and Bronner, 2012). Data from animal models suggest that emigrating NCCs upregulate

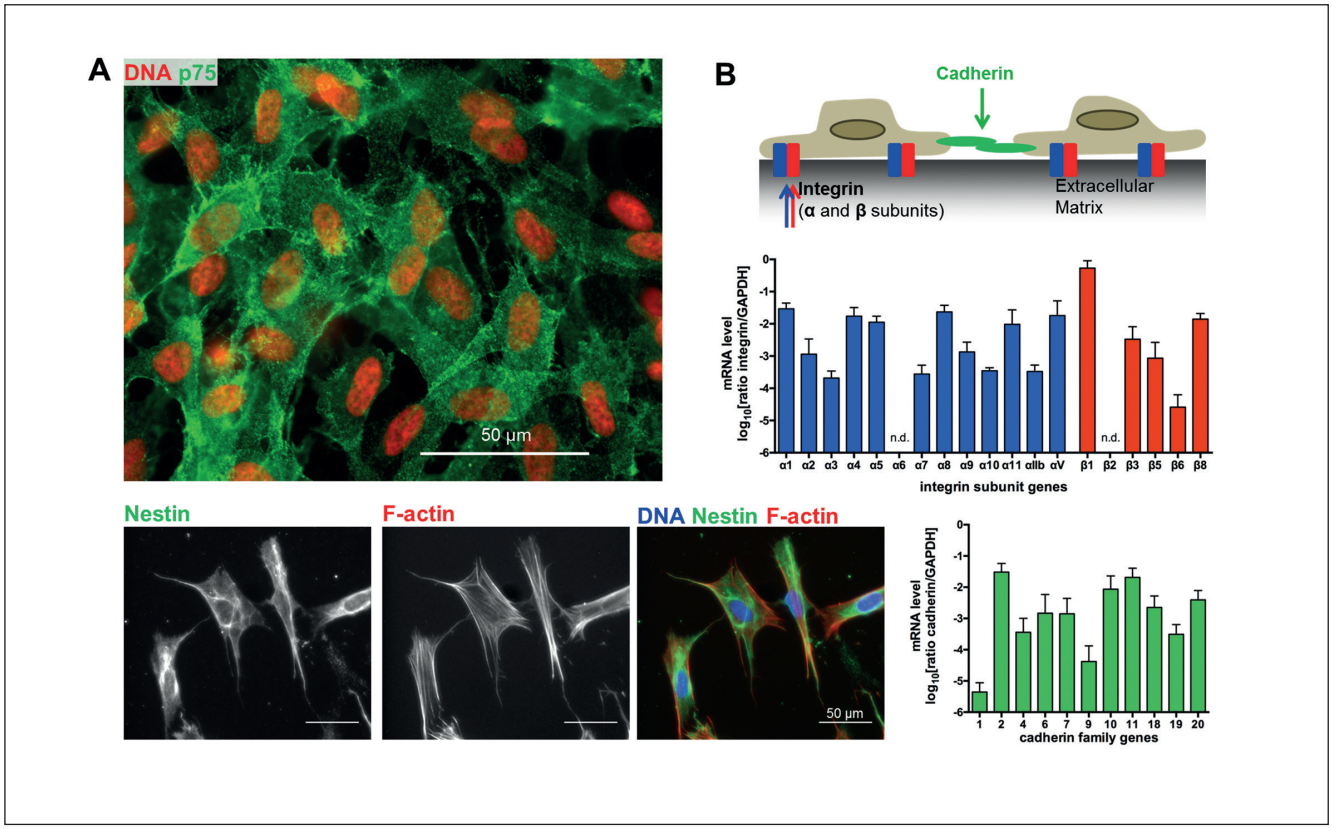

Fig. 1: Characterization of the test system

(A) Cells were plated under standard assay conditions, fixed after 24 h and labelled with immunofluorecent antibodies against the low affinity nerve growth factor receptor (p75, upper image). Alternatively, cells were double-stained for nestin and F-actin (lower image). The scale bar corresponds to 50 µm. (B) NCCs plated for 72 h were profiled for the gene expression pattern of cell adhesion molecules by qPCR analysis. The expression levels of different integrin genes (e.g., β1-integrin = "β1") or cadherins (e.g., CDH2 = "2") are presented as ratios over the expression of the reference gene GAPDH. Note the log10 axis scaling, i.e., up to 10,000-fold expression differences between members of the same gene family. Data are means ± SD of four cell batches. N.d., not detectable with at least two different primer pairs.

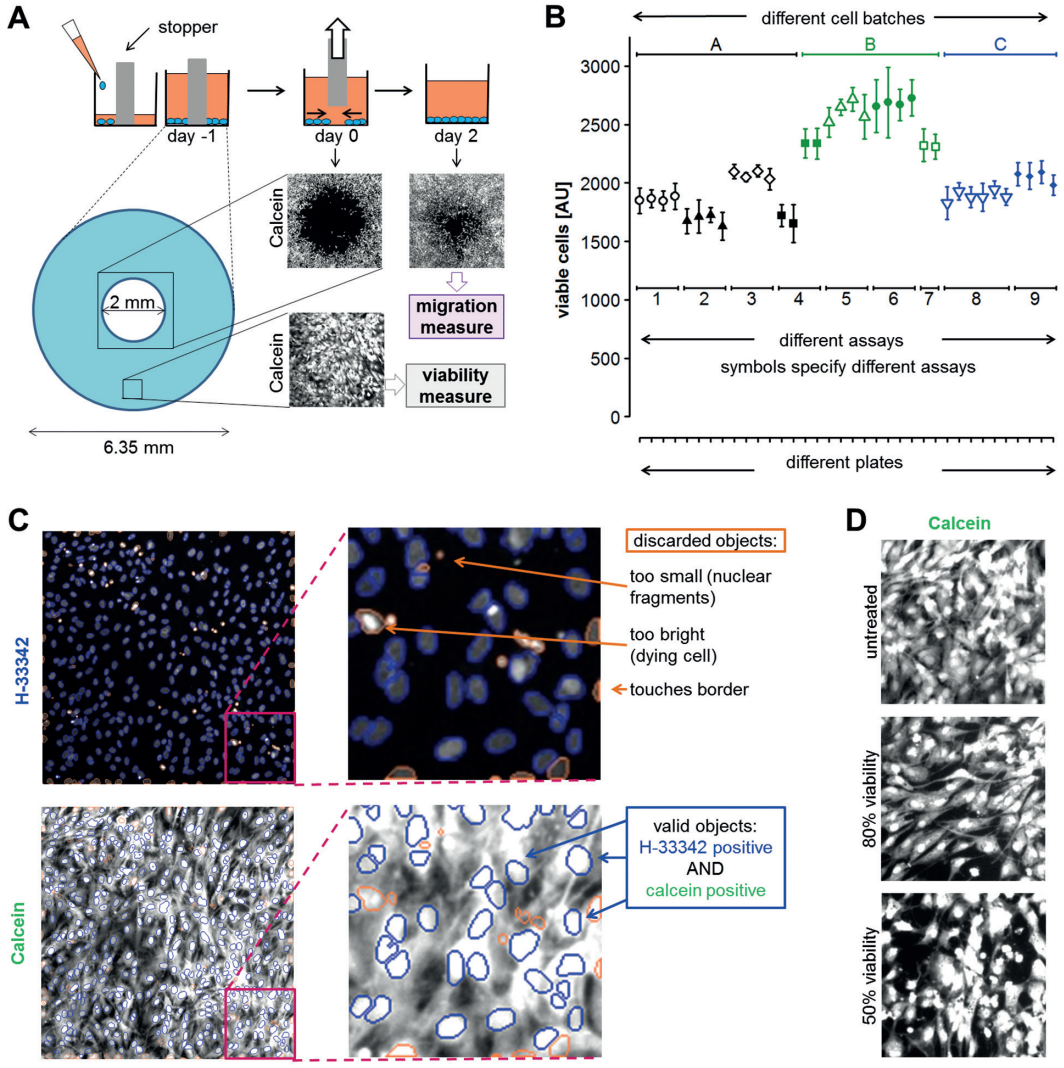

Fig. 2: Assay principle and determination of cell viability

(A) For the standard assay setup, cells were seeded in wells containing silicone stoppers to create a cell-free circular area. One day after the seeding of the cells, the stoppers were removed and the cells were allowed to migrate into this circular area for 48 h. Then, the central circular area was imaged to assess cell migration, whereas images from the outer part were taken to measure cell viability. (B) To obtain data on the variability of plating and on the range of cell densities, the number of viable cells was counted (on day 2) in image fields of standardized size outside the migration area. Variations between plates, assays and cell batches are displayed. AU, arbitrary units (= cell count per unit area). (C) Schematic explanation of the algorithm used to evaluate cell viability: image information was used both from the H-33342 and the calcein staining pattern within the same image. In a first step, the H-33342 channel was analyzed, and the cell nuclei were segmented. Nuclei that either touched the border, were too small (nuclear debris of dead cells) or too bright (dying/apoptotic cells) were excluded (marked in orange). In a second step, information from calcein staining of the same field was used. The algorithm evaluates whether the calcein stain that co-localizes with the respective nuclear area is above a defined threshold, and thus the cell belonging to this nucleus is defined as viable (marked in blue). The pictures to the right are magnifications of the indicated cell area (in red) on the left. (D) Typical examples of image data related to viability measurements: untreated cells formed a dense cell layer, whereas cells treated with 100 or 200 µM chloroquine for 24 h (80% and 50% viable cells compared to untreated controls) were less dense and displayed more apoptotic nuclei.

CDH7 (in birds), CDH6 (in mouse), and CDH11 (in mouse and *Xenopus*) (Kimura et al., 1995; Nakagawa and Takeichi, 1995, 1998; Inoue et al., 1997; Vallin et al., 1998; Strobl-Mazzulla and Bronner, 2012; McKeown et al., 2013). Moreover, CDH2, CDH6, CDH9 and CDH11 are expressed by mouse vagal enteric NCCs (Breau et al., 2006; Heanue and Pachnis, 2006; Vohra et al., 2006; McKeown et al., 2013). This suggests that the human NCC generated here have a cadherin expression pattern consistent with their NCC identity, but it needs to be noted that different NCC populations in animals (along the rostral-caudal, and along the developmental timing axes) can have differing cadherin patterns.

In summary, this biological characterization of the test system, based on the set of cell adhesion molecules and the cytoskeletal phenotype, is well in agreement with the NCC being a migratory cell population suitable for test development.

3.2 Assay principle and determination of cell viability

The NCCs were used to establish a migration assay based on the principle that cells were plated around a silicone stopper in a culture dish and were allowed to move into the circular cell free zone (2 mm diameter) upon removal of the obstacle. After 48 h, the number of cells that had migrated into the circular target zone was quantified. Staining of cells with H-33342 and calcein-AM allowed counting of the total number of migrated cells. Moreover, recording of images in the same well but outside the migration zone allowed a robust and absolute (independent of control measures) quantification of the cell viability, e.g., after treatment of the cells with toxicants (Fig. 2A).

As the number of migrated cells depends on various assay conditions, such as the number of plated cells, it was interesting to obtain a measure of the variability of cell numbers in the assay. We observed up to twofold variations between cell batches (most likely due to the freezing conditions, and the differing proliferation rates of the lots). The variation of the number of plated cells between assays (using cells of the same frozen lot) was usually below 20% (due to, e.g., varying plating efficiency and small differences in proliferation during the assay time (72 h altogether)); the variation between plates within one assay was < 5% (Fig. 2B), and the same was observed within one plate (not shown). This was deemed suitable for our approach of referring the number of cells in the migration zone to the number of cells in controls measured on the same plate, and in the same assay.

For the analysis of viability and migration, a previously published staining procedure as well as the cognate evaluation algorithm (Stiegler et al., 2011; Krug et al., 2013a; Hoelting et al., 2016) were adapted to NCC. Co-staining of nuclei with H-33342 and the overall cells with calcein–AM allowed segmentation and classification of the stained objects, as being: cell debris, dead cells (e.g., apoptotic cells) or viable cells (calcein-positive cell nuclei) (Fig. 2C). Untreated cells formed a dense cell lawn that was strongly calcein-positive. If cells were treated with a cytotoxicant, the number of stained cells decreased (Fig. 2D), and this loss could be quantified by using information from the H-33342 channel of the same field. The proposed setup thus allowed measurements of migration and viability in the same well. This is important as small impairments of viability can seriously affect migration.

3.3 Generation of software for image processing related to the NCC migration assay

In our assay, migration was defined as the number of viable, i.e., H-33342 and calcein double-positive, cell nuclei in the migration zone. To obtain such data, a number of complex steps was required. To make this process at the same time traceable and less resource (operator time)-demanding, we developed a program with a graphical user interface (GUI) and automated standardized procedures that can be downloaded from our website (http://invitrotox.uni-konstanz.de/). The first problem solved by the software is the positioning of the "migration zone" in the image field. Alternative approaches would have been to assume the same central position (but in practice there is variation in the position of the silicone stoppers), or to image the cell layer before and after migration (but this would require fluorescent labelling of the cells before the assay and this manipulation might affect their function). After positioning of the region of interest (ROI, "migration zone"), the software counts the number of viable cells in this ROI. This process is supported by the GUI, which allows the user to set optimal parameters for image segmentation (Fig. 3).

This procedure allowed a half-automated evaluation of migration for a 96-well plate. Usually parameters were adapted for each plate, as the calcein signal sometimes varied between plates (e.g., due to incubation time). Importantly, the software allowed a quick visual control of all ROI on the plate. This was always used for a reality check and wells with badly positioned ROI were excluded. The latter happens, e.g., when cells are plated inhomogeneously or when the illumination of the imaging field is uneven. For practical purposes, it is also important to know that the segmentation fails if cells are plated too densely (overlapping nuclei of migrated cells) or if most of the cells in the migration zone are dead. Under such conditions, no reasonable migration data can be obtained from the assay, and the reality check by the operator, as offered by the software (required time = 1-2 min), can reduce the likelihood of artefactual data from technically poor assays. In a typical experiment, not more than five wells (< 8%) were excluded per plate.

3.4 Preliminary evaluation of ring assay performance using exposure conditions (48 h exposure) similar to the scratch assay

In the previously published wound healing assay, cells were seeded and grown for two days before a scratch wound was introduced. Then toxicants were added and cells were allowed to migrate for 48 h (Zimmer et al., 2012; Dreser et al., 2015). We maintained the 48-h toxicant exposure period in the new assay format, but we introduced a small modification: to avoid well-to-well variations in the cell number at the start of the assay (due to 48 h of proliferation), we slightly modified the protocol by plating higher cell numbers (95,000 cells/cm^2 instead of 66,000 cells/cm^2) and initiating toxicant exposure and migration one day after plating (Fig. S3A, https://doi.org/10.14573/altex.1605031s). The performance of the new migration assay, as to the detection of

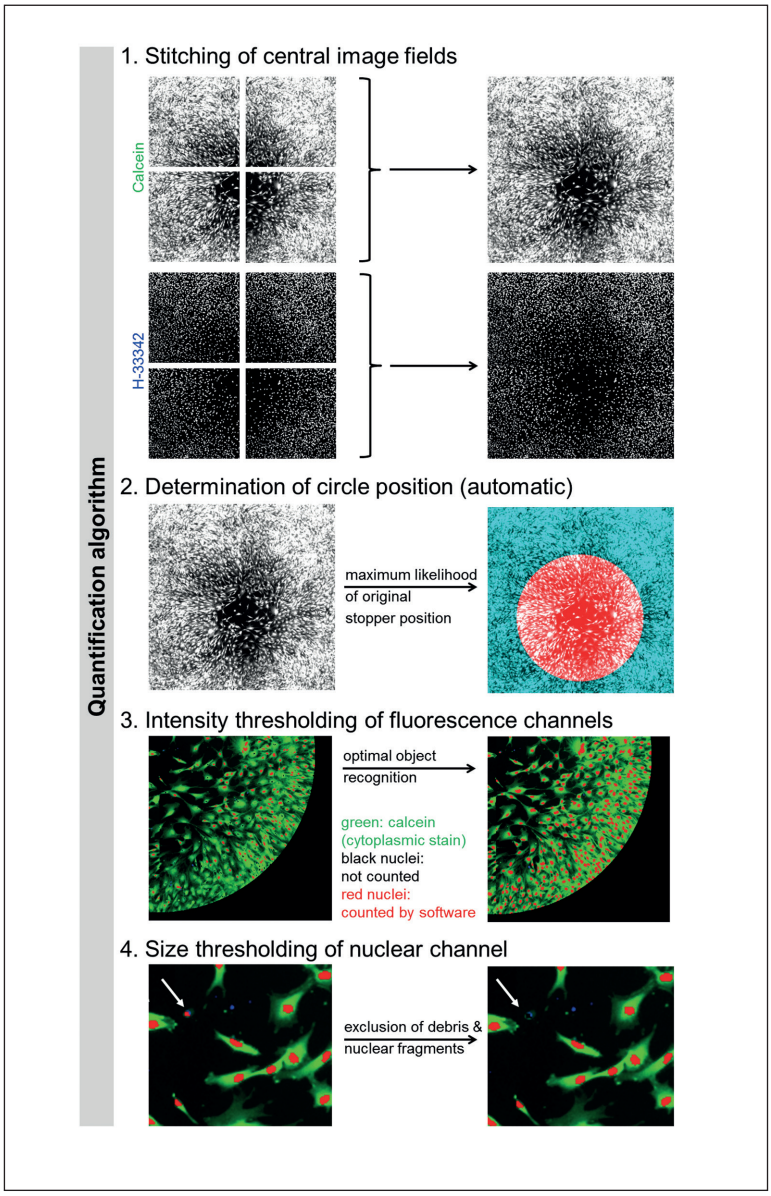

Fig. 3: Image processing steps performed by dedicated NCC migration software

A program was developed to use automatically acquired image data for extraction of quantitative information on migration behavior. In a first step, four images (about 1295 x 1295 µm size; H-33342 and calcein channel) were recorded from the center of the well (96-well dish) with a 5x lens. The four images were joined together to a single image representing a 2590 x 2590 µm square field (1024 x 1024 pixels with our camera settings). In this field, the most likely original stopper position (= "migration zone") was determined automatically by an algorithm that searched for the minimum of signal intensity in the green channel. In a third step, image features were optimized for this migration zone in a user-guided semi-automated way. For instance, threshold and brightness were adjusted manually for both fluorescence channels in a control image. The parameters were considered optimal if each viable cell (green) contained a recognized nucleus (red). The same parameters were then applied by the software to the images from all wells, and the individual cells were identified and quantified automatically (using standard segmentation procedures). Cell debris and nuclear fragments of dying cells were excluded automatically from analysis by setting a minimal threshold for nuclear size.

toxicants, was initially tested with two positive controls: cytochalasin D (CytoD) interferes with actin microfilaments and taxol inhibits microtubule dynamics. Both compounds attenuated NCC migration at concentrations (100 nM; 10 nM) that were non-cytotoxic (Fig. S3B). For this initial, rough evaluation, we adopted benchmark values that had proven useful in other studies (Zimmer et al., 2014; Dreser et al., 2015). For viability, a maximal variation of ≤10%, i.e., a reduction from 100% to 90% was deemed acceptable. Within this range, the variation can be attributed to variation of experimental parameters, while changes beyond this range have a high likelihood of affecting cell functions. For migration, we used the previously determined benchmark value of 75% (Zimmer et al., 2012). The underlying rationale was in part biological plausibility (i.e., meaningful extent of reduction), and in part statistical considerations (all positive controls showing reduction > 25%).

In a next step, two environmental toxicants known to inhibit NCC migration in the original MINC assay (Dreser et al., 2015) were tested. Both As_2O_3 and $CdCl_2$ inhibited migration in the high nM range, but it was not entirely clear whether this effect could be distinguished from general cytotoxicity (Fig. S3B). For all data points at which migration was reduced by more than 25%, viability was reduced by more than 10%. Possibly, different choices of test concentrations may have identified a narrow concentration range in which specific effects on migration occur (> 25% reduction at > 90% viability). For the purpose of the initial evaluation it was sufficient to see that the toxicants showed some tendency to be detected, but were not easily (broad effective concentration range) identified. Note that data stems from three independent experiments.

Fetal bovine serum was found to increase migration in a concentration-dependent manner (Fig. S3C), indicating that the

assay is capable of identifying not only migration-inhibiting but also migration-promoting agents. As a further mechanistic test compound, we used the cytostatic drug AraC to investigate effects of toxicants that affect cell proliferation. AraC affected the migration endpoint (apparently reduced migration), but it also reduced the overall number of viable cells. This indicated that compounds that strongly affect cell proliferation may appear as migration inhibitors and require special attention (Fig. S3C).

Finally, two typical toxicants were tested that have not been used in the MINC before, but where literature data indicate that they could affect NCC migration: acrylamide affected the function of immature neurons derived from NCC (Hoelting et al., 2016) and may therefore also affect NCC function; LiCl affects the migration of other cell types (Wang et al., 2013; de Araujo et al., 2016) and it was therefore a candidate for effects in the MINC assay. In fact, the environmental toxicant acrylamide was specifically migration-inhibiting at concentrations around 1 mM (similar to its effects on neurons), and lithium chloride, a drug used for mood disorders, inhibited migration at a concentration of about 10 mM, similar to its inhibitory effect on glycogen synthase kinase-3 (Bain et al., 2003; Selenica et al., 2007) (Fig. S3D).

The initial evaluation showed that the new test system is able to detect migration-modulating compounds, but for some compounds there may be only a narrow concentration window to identify specific effects. Furthermore, the data obtained with the proliferation inhibitor AraC suggested that the issue of cell proliferation deserved further scrutiny.

3.5 The role of cell proliferation in the 48-h exposure protocol

To investigate proliferation in the 48-h setup in more detail, NCCs were exposed to EdU during the migration phase. This thymidine analog is incorporated into the DNA of proliferating cells, and it can be easily visualized by coupling to a fluorophore. This EdU stain, when combined with H-33342 (staining all nuclei) allowed the discrimination of cells that had undergone replication (S-phase) during the period of EdU exposure (double-positive) and cells that had not proliferated. We found that approximately half of the cells were EdU-positive after 48 h incubation (Fig. S4A, https://doi.org/10.14573/altex.1605031s). An exact quantification (eight separate experiments, based on four different cell lots) showed that 61.6 ± 10% of the cells (means ± SD) were EdU-positive (Fig. S4B). This means that up to 45% of the NCCs present at the beginning of the assay proliferated during the 48-h assay period (the mathematical calculation of this number is based on the assumption that each cell division yields two EdU-positive cells from one original cell). This data, based on EdU incorporation is consistent with our data on cell doubling time (about 70 h) obtained by cell counting. The contribution of cell proliferation to the number of cells in the migration area provides a strong biological rationale for potential misclassification of compounds that affect cell proliferation.

To test directly whether toxicants affected proliferation at concentrations that apparently reduced migration, we measured their effect on EdU-incorporation. For instance, LiCl did not affect EdU incorporation, whereas As_2O_3 and $CdCl_2$ both reduced EdU incorporation by about 40% (Fig. S4C). We also tested whether the apparent enhancing effect of FBS on migration may be due to the stimulation of proliferation. However, this was not the case (Fig. S4C).

Having established that some compounds do inhibit proliferation, and may therefore be falsely classified as migration inhibitors, we used a different technical approach to directly assess mitosis events in the migration zone: cells were observed by video time-lapse microscopy in the migration zone. The two migration-inhibitors used as positive controls, cytochalasin D and taxol, did not significantly affect proliferation, and neither did LiCl. In contrast, $CdCl_2$ treatment significantly reduced replication by about 40%. This corroborated the data obtained with population-wide measurement of EdU incorporation. Treatment with the anti-mitotic agent AraC blocked proliferation nearly completely. Only 3.1% of cells arose from mitosis under this condition, and all the observed cell divisions happened in the first 18 h after AraC addition (data not shown), indicating that these cells probably had started proliferation before AraC addition. Addition of FBS led to a slight, non-significant increase in the proliferation rate. This observation also corroborated the data obtained from EdU incorporation experiments (Fig. S4D).

We conclude from these observations that the cMINC can give alerts on compounds that impair NCC mobility; but our experiments (measurement of EdU incorporation; addition of AraC) also showed that cell proliferation contributes up to 25% of the cells in the migration zone. Therefore, toxicants that affect proliferation, but not migration, may be falsely classified as migration inhibitors. In the following, the protocol was modified to render the assay more specific.

3.6 Optimization of the cMINC assay protocol

To reduce the effect of toxicants on viability and cell proliferation, a shorter toxicant exposure would be favorable. Therefore, we explored a new exposure scheme that exposed the cells to toxicant only during the last 24 h of migration (Fig. 4A). Under these conditions, as before, cytochalasin D and taxol reduced the number of cells in the migration zone and FBS increased it (Fig. 4B). Alternatively, cells were exposed during the first 24 h of migration, and the assay was ended by measurement of viability/migration. This modification did not improve the assay results and was not pursued further (data not shown).

During the optimization experiments, it became evident that there was always a particularly high cell number at the outer rim of the migration zone. We hypothesize that these cells entered the ROI either (i) by "free" migration, (ii) by being "pushed" by the expanding cell layer outside the zone, or (iii) by proliferation of cells bordering the migration zone. Only the first driving force was relevant to our test endpoint, while the other two increased the level of the background signal. Therefore, it was desirable to "cut" the outermost rim from the migration zone. This was achieved by introducing a feature to our quantification software that allows choosing the radius of the migration zone. As the radius of the original silicone stopper was 1 mm, choice of a migration zone radius of 0.9 mm cut out the outermost rim (Fig. 4C). In a control experiment (untreated cells), we tested the influence of radius settings on the number of cells detected in the ROI after 24 h and 48 h. After 24 h of migration, approxi-

mately 400 cells were in the 1 mm radius ROI. When the radius of the ROI was reduced from 1 mm to 0.7 mm, only few cells were present in the ROI. This number then increased strongly during the following 24 h (Fig. 4C, red line). Also, when the radius was only reduced by 100 µm (Fig. 4C, blue line), less than 200 cells were present in the ROI after 24 h, and this number increased steeply (3-fold) within the next 24 h. Thus, reduction of the radius of the ROI allowed elimination of cells entering the migration zone unspecifically, and it allowed a focus of the assay on cells that entered especially during the last 24 h (i.e., during the treatment period). For all following experiments, the size of the ROI was chosen so that it contained at least 150 but not more than 300 cells for control conditions. This radius setting (mostly using values of 0.7-0.85 mm) was done in the same way for all wells of a plate after initial settings by the operator on the GUI.

Using this new setup, concentration-response curves were obtained for several groups of compounds (Fig. 4D-E and Fig 5). In agreement with the results of 48 h exposure, cytochalasin D

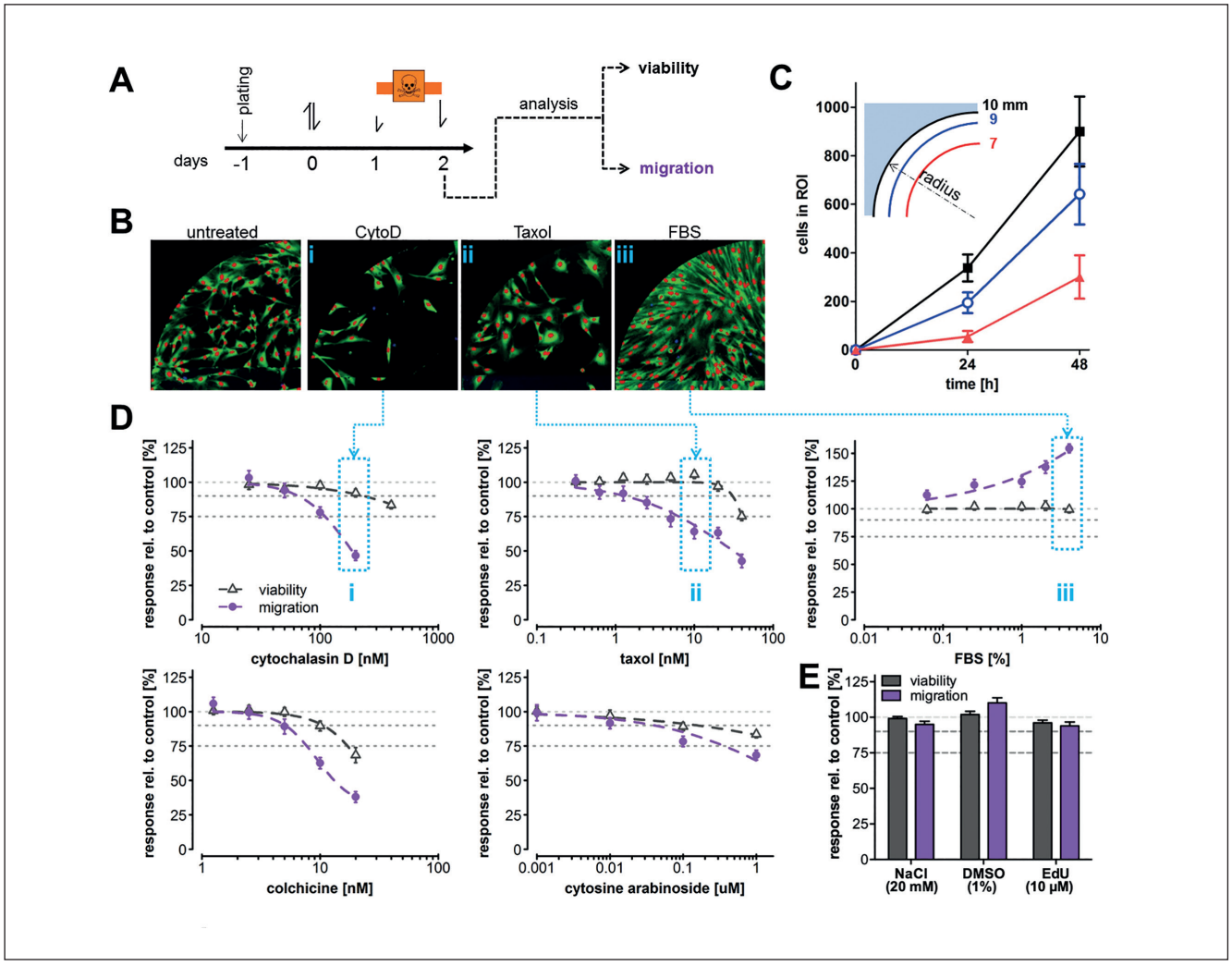

Fig. 4: Setup of optimized circular MINC (cMINC) assay (with 24 h toxicant exposure)

(A) Schematic indicating the altered exposure scheme: cells (plated at 30,000/well) were allowed to migrate from day 0 to day 2; toxicant exposure was from day 1 to day 2 (only last 24 h). (B) Representative images of the "migration zone" (one quarter of the circular zone is shown at the end of the experiment) after exposure to three (i-iii) positive controls that enhance or inhibit migration. The cell cytoplasm is depicted in green (calcein); nuclei, positive for both H-33342 *plus* calcein are depicted in red. (C) To quantify the migration, a new feature was added to the software, so that it allowed to set the radius of the regions of interest (ROI) to be used for scoring of migrated cells. Data from an exemplary experiment show how many cells were detected in the ROI 24 h and 48 h after removal of the stopper (with examples for different radius choices shown). (D) Concentration-response curves were obtained from mechanistic calibration compounds (endpoint-specific controls) under the new cMINC conditions. All values are normalized to untreated controls. Three exemplary situations corresponding to the images shown in B are highlighted (i, ii, iii). (E) Measurements of viability and migration for negative control compounds. The light gray dotted line indicates the 100% y-axis value for easier reading of the diagrams. The other two dotted lines are drawn at 90% (indicating threshold for reduced viability) and at 75% (indicating the threshold for reduced migration). Data are means ± SD, n = 3.

and taxol inhibited migration and FBS increased migration (Fig. 4D), although FBS was less effective than in the 48-h setup. Colchicine, a microtubule polymerization inhibitor also inhibited migration in the nM range. (Fig. 4D). The cytostatic drug AraC had less pronounced effects than in the 48-h setup, and it would now definitely not be scored as a migration inhibitor.

The obtained results were verified by time-lapse video microscopy and tracking of individual cells (Fig. S5, https://doi.org/10.14573/altex.1605031s). Cytochalasin D and taxol both decreased the distance covered by cells within 24 h (i.e., the speed of individual cells), whereas FBS had the opposite effect. The proliferation inhibitor AraC did not affect cell speed. Thus, the different analytical approach of direct tracking of migrating cells over the full assay time fully corroborated the results obtained with the "fixed time point" cMINC assay.

The negative controls NaCl, DMSO as well as EdU did not affect viability and migration (Fig. 4E).

Testing of a variety of developmental toxicants under the new cMINC conditions suggested that As_2O_3 and $CdCl_2$ inhibit migration; this effect was more distinct than in the 48-h setup (Fig. 5A). Acrylamide and LiCl had a wider concentration window, but the potentially specific concentration range of acrylamide was still narrow compared to that of $CdCl_2$ or LiCl. Polychlorinated biphenyl (PCB)180, a known NCC migration inhibitor (Dreser et al., 2015), strongly inhibited migration in this setup (even more effectively than cytochalasin D and taxol). Further-

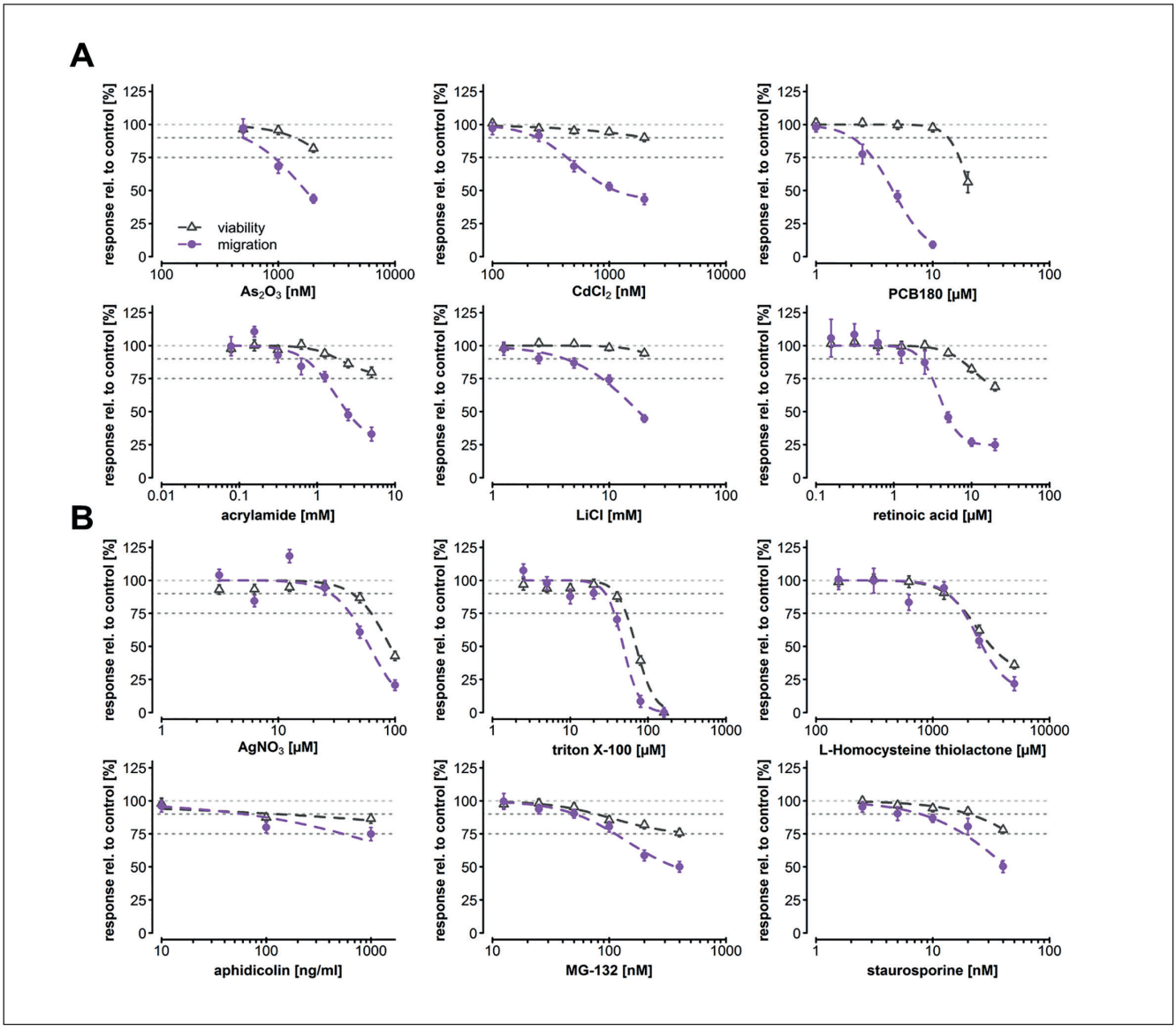

Fig. 5: Assay performance of optimized circular MINC (cMINC) assay (24 h toxicant exposure)

Cells were plated (30,000/well) and migration was initiated by removal of the stoppers one day later (as in Fig. 4A). Concentration-response curves of viability and migration from (A) exemplary test compounds; and (B) generally cytotoxic compounds with no specific effect on migration inhibition. Data are means ± SD, n = 3.

more, another migration-inhibiting compound was identified: the teratogen retinoic acid inhibited NCC migration at µM concentrations (Fig. 5A). Similar data were obtained with cells of different origin, such as human iPSC lines (Fig. S2).

Finally, we explored the effect of unspecific toxicants on the test system endpoints. The cytotoxicants Triton X-100 (detergent), $AgNO_3$ (toxic metal), and L-homocysteine thiolactone (toxic metabolite found in human neurological disorders) reduced the migration endpoint, but they also reduced cell viability at similar concentrations (Fig. 5B). From the comparison of the endpoint curves, we would conclude that such compounds are not specific inhibitors of NCC migration. We also tested another proliferation inhibitor, the DNA synthetase inhibitor aphidicolin (Fig. 5B). Like AraC, it only produced a minor effect. Other cytotoxicants tested were the proteasome inhibitor MG-132 (Grimm et al., 1996; Qiu et al., 2000) and the universal apoptosis inducer staurosporine (Weil et al., 1996; Nicotera and Leist, 1997). Here, the concentration-response curves of viability and migration also separated only to a small extent (Fig. 5B).

In conclusion, the new 24 h cMINC assay protocol allowed a better separation of migration inhibitors from compounds that indirectly affected migration through effects on viability and/or proliferation.

3.7 The role of proliferation for assay outcome in the optimized cMINC

The fact that AraC affected migration also in the 24-h setup suggested that proliferation still played a role. To quantify this, EdU incorporation was measured, and about half of the cells (exactly 52%) in the migration zone were found to be EdU positive (Fig. 6A). This means that one third of the cells that entered the migration zone during the assay divided during the 24 h of the assay period. Moreover, this means that only 75% of the cells present at the end of the assay were present before toxicant addition (Fig. 6B). If a compound inhibited all proliferation (like AraC) it would thus reduce the final cell number by 25%. This would be measured as a viability of 75% (number of cells compared to untreated controls), and as an inhibition of migration by 25% (i.e., a cell number in the migration zone of 75%, compared to controls), in parallel with the overall 25% reduced cell number. This consideration is corroborated by experimental data obtained from cells treated with AraC. Exposure of NCCs for 24 h with 1 µM AraC resulted in 80% viability and approximately 75% of migration (Fig. 4D). Thus, a reduction of migration by > 25% is unlikely to be explained by effects on proliferation.

We used a large variety of treatment conditions to explore whether there was any correlation of reduced proliferation with reduced migration in the cMINC assay. EdU was added during the treatment period. At the end of the test, viability and migration were measured following the standard protocol, and afterwards cells were fixed, stained and scored for EdU (in the cell layer outside the migration zone). Proliferation and migration did not correlate (Fig. 6C). Three different scenarios were observed: (I) conditions that inhibited proliferation but not migration. Compounds in this group comprised the proliferation inhibitors AraC and aphidicolin as well as MG-132 and staurosporin (Fig. 6C, group I in black); (II) Conditions that inhibited migration but not proliferation. This group comprised cytochalasin D, taxol as well as PCB180 (Fig. 6C, group II in blue); (III) conditions that affected both proliferation and migration. High concentrations of LiCl, $CdCl_2$, and acrylamide and low concentrations of colchicine fell into this third group (Fig. 6C, group III in red).

For the last group of conditions (group III), it cannot be ruled out that the observed inhibition of migration is caused partially by inhibition of proliferation. To get more clarity on the effects of such compounds, the cMINC was performed in the presence of AraC in controls and in all treated samples to eliminate proliferation. Aphidicolin was measured under the same conditions as an example for group I. There was no effect on viability or migration (Fig. 6D), in contrast to data obtained in the absence of AraC (Fig. 5B). This showed that the apparent cytotoxicity of aphidicolin under control conditions was in fact due to a diminished cell number as a result of reduced proliferation. Cytochalasin D, a compound of group II, also inhibited migration when co-treated with AraC (Fig. 6D). Therefore, cytochalasin D can be considered a "true migration inhibitor", i.e., acting also under conditions when proliferation does not play a role. Such data might suggest that the cMINC should always be performed in the presence of AraC. This altered protocol may result in the reduction of noise, an improved baseline, and the avoidance of artifacts caused by compounds that attenuate cell proliferation. However, it may also be argued that such a test setup also has disadvantages, as cells would be exposed to a known toxicant (AraC), and there may be interactions between this compound and the test compounds that cannot be anticipated. Our suggestion for a testing strategy is to perform the cMINC without addition of AraC for the initial screening of compounds. Problematic compounds (unclear effects; only partial separation of viability and migration curves; evidence or suspicion of inhibited proliferation) would then be re-tested, e.g., in the modified cMINC in the presence of AraC. Such a sequential approach is in agreement with the concept that the results from a screening assay (as the cMINC) can never be taken as definitive toxicological proof without further confirmation.

We tested such an approach, using some of the compounds in group III (ambiguous conditions). Acrylamide, $CdCl_2$, LiCl and colchicine all inhibited migration in the cMINC with AraC in at least one concentration that did not reduce viability (below 90%). For instance, 20 mM LiCl, a condition that gave ambiguous results in the absence of AraC (Fig. 5A), clearly inhibited migration in the AraC-modified cMINC without causing cytotoxicity (Fig. 6D). Potency and efficacy of some compounds were altered by testing in the presence of AraC. As these shifts were relatively moderate, we consider this an additional reason to use AraC-free conditions for standard testing, and follow up with an AraC-modified cMINC when inhibition of proliferation is suspected (e.g., reduction of cell number at the end of the assay without evidence for cell death).

3.8 Construction of preliminary prediction models for the optimized cMINC test

During test development, we used semi-quantitative estimates of test outcome, such as visual comparisons of curve shapes or positioning of point estimates of data relative to benchmark

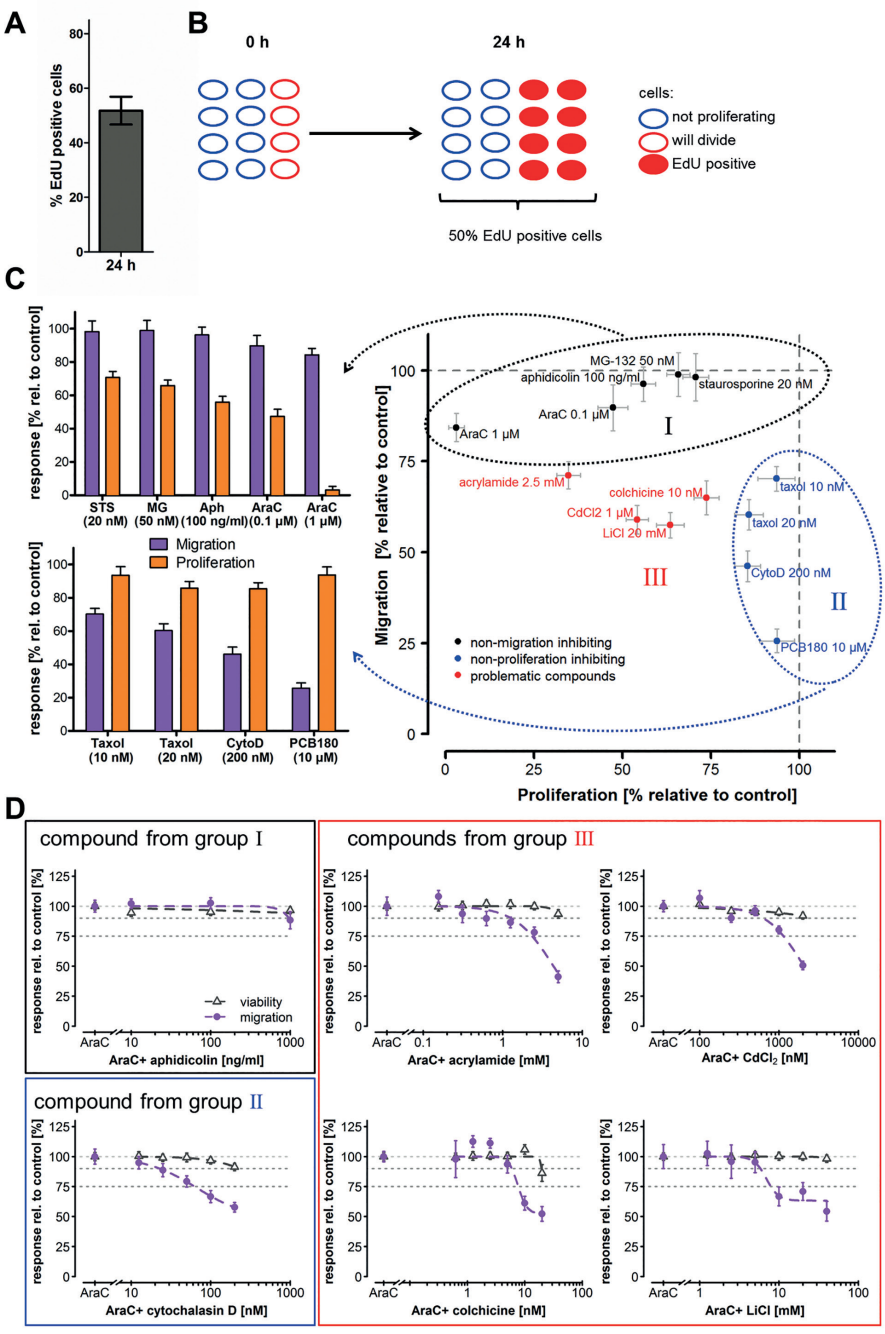

Fig. 6: The role of cell proliferation in the new cMINC assay format

Cells were plated (30,000/well) and migration was initiated by removal of the stoppers one day later (as in Fig. 4A). After 24 h, test compounds were added and assay endpoints were assessed 24 h thereafter. (A) Cells were incubated with EdU (10 µM) during the last 24 h of the assay, and the number of EdU and H-33342 double-positive cells was quantified (means ± SD; n = 3). (B) A schematic diagram illustrates the relation of dividing cells and cells incorporating EdU: 50% of EdU positive cells will arise if one third of the cells divides over a 24 h period. (C) Relationship between cell proliferation (assessed by the incorporation of EdU (10 µM)) and apparent cell migration (assessed in the cMINC assay): some exposure conditions inhibited proliferation but not migration (upper bar graph, black group in scatter plot). Under some conditions, migration was inhibited, but not proliferation (lower bar graph, blue group in scatter plot), and some affected both endpoints (red group). (STS, staurosporine; MG, MG-132; Aph, aphidicolin; AraC, cytosine arabinoside) (D) Concentration-response curves for viability and migration in the presence of the proliferation inhibitor AraC (1 µM) for selected compounds of the three different groups in (C). All values are normalized to cells treated with 1 µM AraC only. Data are means ± SD from three independent experiments.

values (90% viability; 75% migration). Finalization of test development and objective classification of compounds require a prediction model. A suitable prediction model has to take into account that the cMINC assay measures two endpoints simultaneously: migration and viability. One solution for other assays with two endpoints (e.g., neurite outgrowth) has been to calculate the ratio between effective concentrations (EC) of both endpoints (Stiegler et al., 2011; Krug et al., 2013a; Hoelting et al., 2016; Ryan et al., 2016). For example, Stiegler et al. used the ratio of EC50 of viability to EC50 of neurite outgrowth; Ryan et al. used the ratio of benchmark concentrations (BMC) for viability to neurite outgrowth. Although this approach has proven beneficial in these cases, it is less suitable for the cMINC assay for several reasons: (i) some compounds do not affect viability at all in the testable concentration range; (ii) some compounds substantially affect migration, but the determination of a meaningful EC50 value is problematic for mathematical reasons because of the curve shape; (iii) migration requires the contribution of multiple signaling pathways, and inhibition of any one of them only partially impairs cell migration (Zimmer et al., 2012). This results in curves that have asymptotes at, e.g., 70, 50 or 30% migration capacity, or that do not have an asymptote at all, as increasing toxicant concentrations activate different mechanisms of toxicity. This uncertainty in curve fitting may create uncertainties for benchmark values also in the upper part of the curve (e.g., for determination of BMC10 or BMC15 values). We therefore decided to establish various candidate prediction models (PM), to compare their performance, and to pick the best-suited PM for more extensive evaluation in follow-up studies.

We used sixteen compounds for the initial evaluation. These comprised 9 positive controls and 7 compounds assumed to have no specific effect on migration (unspecific controls). A good PM would classify the 9 positive controls as "specific migration inhibitors" and the other seven compounds as "non-specific toxicants". We used fixed benchmark values of 90% and 75%. The 90% cutoff is a commonly used value, based on biological plausibility that changes in a viability parameter below this value may not be meaningful. The 75% cutoff for migration is based on our findings that artefacts due to inhibition of proliferation may cause up to a 25% change of migration, but not more (Fig. 6). An alternative approach to the choice of fixed values would have been a determination based on the noise of the background signal (e.g., 3 x SD of solvent controls). In practical terms, such an approach (Ryan et al., 2016) would have yielded relatively similar cutoffs, not far from the 90% and 75% values. We preferred the fixed value approach here for its anchoring to biological plausibility, instead of test statistics. For future determinations of a definite PM model, both approaches will be reconsidered.

First, we fitted curves through the viability and migration data and determined an EC90 value, i.e., an effective concentration bringing viability down to 90% ($EC90_V$) and an effective concentration bringing migration down to 90% ($EC90_M$). Ranking the compounds according to the ratio $EC90_V/EC90_M$ did not allow separation of specific and unspecific compounds. Also, other EC-based ratios ($EC75_V/EC75_M$; $EC50_V/EC50_M$) were not useful (Fig. 7A).

Second, we proceeded as in the first approach, but used different benchmark values for migration and viability (e.g., 75%/90%). On this basis, various ratios were calculated. For instance, the $EC90_V/EC75_M$ was used. In this model, a ratio of 1 corresponds to 25% migration inhibition at 90% viability. Compared to the first approach, this PM takes into account that BMCs for different endpoints may be different due to the difference of the underlying biological process or due to differences in baseline noise. Using the $EC90_V/EC75_M$ ratio allowed separation of specific and unspecific compounds (Fig. 7B). All unspecific compounds had a ratio ≤ 1.11, whereas calibration compounds and developmental toxicants reached a ratio of > 1.3. Thus, the $EC90_V/EC75_M$ ratio allowed a separation of the two compound groups, and a threshold value of 1.3 may be used for classification. However, the obtained parameter is unit-less and does not contain information about the efficacy of migration inhibition.

As a third approach, we examined the level of migration inhibition at the no observed adverse effect level (NOAEL) of viability ($NOAEL_V$). This method was used in the previously published wound healing assay (Zimmer et al., 2012). However, the NOAEL depends on the spacing of the data points and hence is not always accurate. To circumvent this problem, we slightly modified the approach and used the level of migration inhibition at the $EC90_V$. This PM also allowed separation of the two compound groups (Fig. 7C). All calibration compounds reached at least 40% of migration inhibition whereas the unspecific compounds only inhibited migration up to 30%. Thus, a threshold value for classification may be set at 30%, but better definitions are possible after testing of a larger group of compounds. Alternatively, a threshold may also be set at 25% migration inhibition. This would correspond to the rough threshold setting in the initial part of our study. Such a decision would decrease the specificity of the assay, but increase its sensitivity. If the assay is performed for screening or to obtain alerts on potential developmental toxicants, we suggest to use the 25% threshold and to follow up with a secondary test.

Complementary to the PM, a ranking of test compounds according to potency is useful for some applications. An overview of the $EC90_V$ values (Fig. 7D) shows that our study was based on a wide dynamic range (six orders of magnitude) of toxicities and still distinguished specific and unspecific migration inhibitors over the full range of general cytotoxicity. As a measure for potency with respect to migration inhibition, we propose the use of the $EC75_M$ (Fig. 7E). Two considerations are important in this context: first, the measure of "migration potency" is only meaningful for compounds that have been defined as migration-inhibitors in a prediction model (e.g., > 25% migration inhibition at the $EC90_V$), and it should not be used for other compounds; second, we decided here to use $EC75_M$ instead of, e.g., $EC70_M$. This follows the precautionary principle of assuming that biologically meaningful effects may already occur when migration is inhibited by 25%.

For further use, we suggest to use both the "$EC90_V/EC75_M$" PM and the "migration at $EC90_V$" PM, and to combine them by defining a hit as when a compound is classified as positive in either of the models. A hit would be followed up by secondary testing (concentration response curve in cMINC with more data

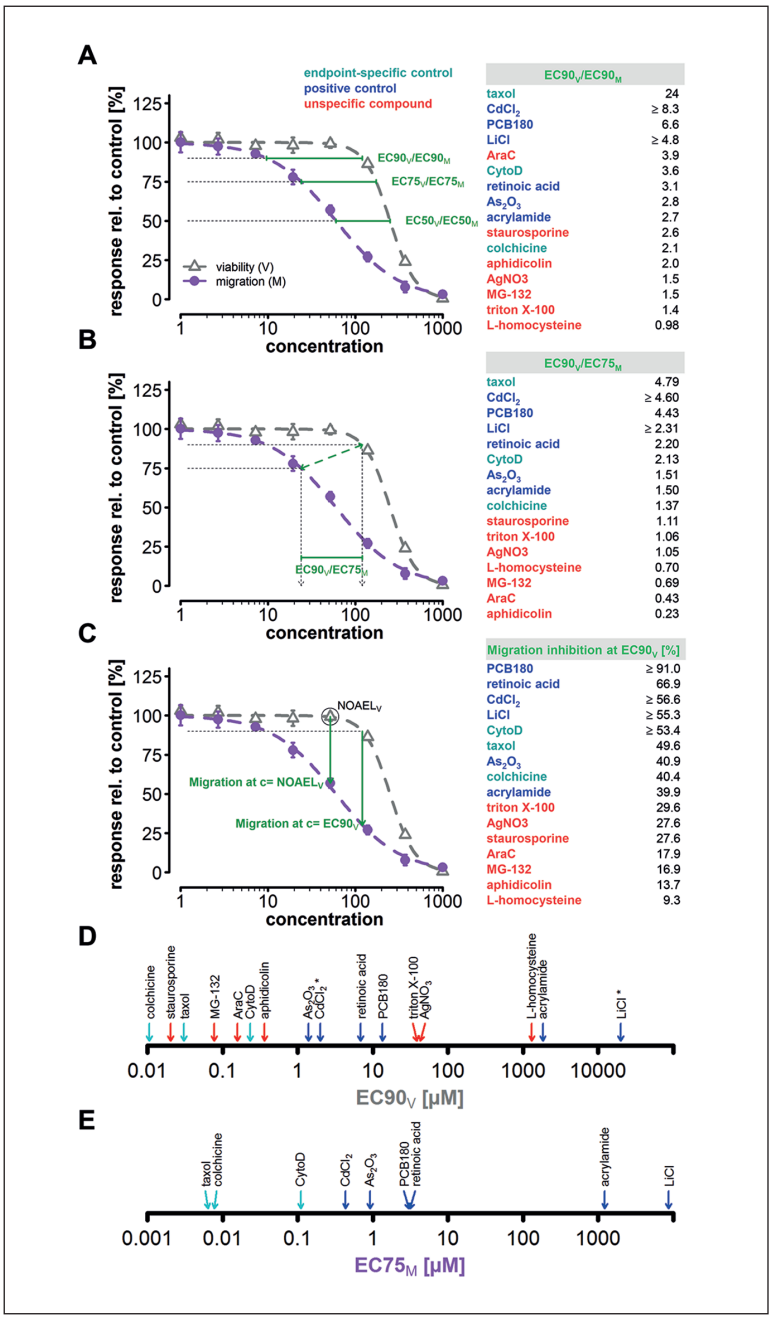

Fig. 7: Preliminary prediction model to classify tested compounds in the cMINC assay
Assay setup and data acquisition were as in Fig. 4; migration (M) and viability (V) were measured for 16 compounds. Endpoint-specific controls are depicted in turquoise, positive control test compounds in blue and negative/unspecific compounds in red. (A, B, C) Schematic representation (on the left) of the parameter used to rank the compounds and the corresponding ranking (on the right). (A) Ratio of EC90 of viability and EC90 of migration ($EC90_V$ = concentration with 90% of normal cell viability; $EC90_M$ = concentration allowing 90% of the full migration). (B) Ratio of EC90 of viability and EC75 of migration ($EC75_M$ = concentration allowing 75% of the full migration). (C) Migration inhibition (= % reduction of migration) at the EC90 of viability or at the no observed adverse effect level (NOAEL) of viability. Note that "adverse" is defined here as reduction of viability by > 10%. (D) Graphical representation of the potency of compounds with respect to effects on cell viability (as EC90 of viability). The asterisk (*) indicates that the real EC90 is higher than the value shown; in these cases, the highest concentration tested is displayed. (E) Graphical representation of the potency of compounds with respect to effects on cell migration (as EC75 of migration).

points; AraC-modified cMINC), a definition of potency, and an estimate of efficacy. To further reduce uncertainty, additional types of migration assays may be used in the future.

4 Conclusions

We successfully established an assay to test for interference with human NCC migration. Proliferation was identified as a potential confounding factor, which can be overcome by repetition of the assay under conditions suppressing proliferation (presence of mitotic inhibitors). Furthermore, we compared the standard migration endpoint with information from video microscopy time-lapse experiments. We established a preliminary prediction model on the basis of these data. The assay has a medium to high throughput (The automated image acquisition and the analysis with a tailored software allow a skilled operator to measure 500-1000 wells/week. This would yield 100-200 data points/week assuming the use of five technical replicates). However, the production of sufficient cells for high throughput testing would be limited by the laborious standard differentiation protocol. An alternative procedure to differentiate NCCs (Mica et al., 2013), as used here for one of the iPSC cell lines, allows generation of NCCs in significantly shorter time.

Concerning the biological relevance of the test system, it needs to be noted that migration occurs *in vivo* in a 3D cellular environment: NCCs perceive chemoattractive and chemorepulsive signals from the surrounding cells and permeate other tissues/cell populations during their migration on defined routes (Theveneau et al., 2013; Green et al., 2015; Shellard and Mayor, 2016). In contrast to this, our test uses a 2D cell free migration zone. It is mechanistically not fully understood why the cells migrate into the cell-free space. One hypothesis is that the underlying mechanism is a non-directed cellular drive for movement. Apparently-directed movement into the migration zone may occur because there are fewer cells in this circular area and thus fewer contact-inhibition signals are perceived. Another hypothesis is that the cells migrate via a "chemotactic mechanism", i.e., that they perceive signal differences between the cell-free space and the populated area. So far, information from the time-lapse experiments agrees best with the first hypothesis, as the cells do not seem to migrate in a directed manner into the cell-free circle. In the future, it would be interesting to model the chemotactic migration of NCCs more closely, and to investigate whether toxicants are able to specifically alter chemotaxis of NCCs.

The classical animal-based approach utilized for developmental toxicity testing comprises the measurement of apical endpoints such as tissue malformations, mortality and growth retardation. This approach has a low sensitivity and specificity with respect to human hazard prediction (Hartung and Leist, 2008; Leist et al., 2008; van Thriel et al., 2012; Smirnova et al., 2014). The evaluation of *in vivo* developmental toxicity testing data indicates a high percentage of false positive (~40%) (Hartung, 2009) and of false negative (~55%) classifications (Bremer and Hartung, 2004). Furthermore, the concordance among different laboratory mammalian species is lower than 60% (Hartung, 2009; Sipes et al., 2011; Leist et al., 2014).

Some of these limitations may be overcome by human-cell based assays, as presented here (cMINC assay) or suggested earlier (Hansson et al., 2000; Scholz et al., 2011; Balmer et al., 2012). At present, the assay shares an important shortcoming with classical animal-based tests: it does not give information on the mechanism of migration inhibition. Toxicants could alter migration via different mechanisms, for example by interfering with cytoskeletal remodeling (i.e., cytochalasin D or taxol), by energy depletion (Volbracht et al., 1999; Latta et al., 2000) or by induction of cell differentiation. Moreover, it remains open whether the identified toxicants inhibit migration via a NCC-specific or a cell-type unspecific mechanism. Addressing such questions will require the combination of mechanism-oriented endpoints (e.g., omics technologies) with our phenotypic test, and extensive comparison to other models.

References

Bain, J., McLauchlan, H., Elliott, M. et al. (2003). The specificities of protein kinase inhibitors: an update. *Biochem J 371*, 199-204. https://doi.org/10.1042/BJ20021535

Bal-Price, A. K., Coecke, S., Costa, L. et al. (2012). Advancing the science of developmental neurotoxicity (DNT): Testing for better safety evaluation. *ALTEX 29*, 202-215. https://doi.org/10.14573/altex.2012.2.202

Balmer, N. V., Weng, M. K., Zimmer, B. et al. (2012). Epigenetic changes and disturbed neural development in a human embryonic stem cell-based model relating to the fetal valproate syndrome. *Hum Mol Genet 21*, 4104-4114. https://doi.org/10.1093/hmg/dds239

Balmer, N. V., Klima, S., Rempel, E. et al. (2014). From transient transcriptome responses to disturbed neurodevelopment: Role of histone acetylation and methylation as epigenetic switch between reversible and irreversible drug effects. *Arch Toxicol 88*, 1451-1468. https://doi.org/10.1007/s00204-014-1279-6

Barczyk, M., Carracedo, S. and Gullberg, D. (2010). Integrins. *Cell Tissue Res 339*, 269-280. https://doi.org/10.1007/s00441-009-0834-6

Barouki, R., Gluckman, P. D., Grandjean, P. et al. (2012). Developmental origins of non-communicable disease: Implications for research and public health. *Environ Health 11*, 42. https://doi.org/10.1186/1476-069X-11-42

Beauvais, A., Erickson, C. A., Goins, T. et al. (1995). Changes in the fibronectin-specific integrin expression pattern modify the migratory behavior of sarcoma S180 cells in vitro and in the embryonic environment. *J Cell Biol 128*, 699-713. https://doi.org/10.1083/jcb.128.4.699

Bennett, D., Bellinger, D. C., Birnbaum, L. S. et al. (2016). Project TENDR: Targeting environmental neuro-developmental risks. The TENDR consensus statement. *Environ Health Perspect 124*, A118-A122. https://doi.org/10.1289/EHP358

Bergeron, K. F., Cardinal, T. and Pilon, N. (2013). A quantitative cell migration assay for murine enteric neural progenitors. *J Vis Exp 79*, e50709. https://doi.org/10.3791/50709

Breau, M. A., Pietri, T., Eder, O. et al. (2006). Lack of beta1 integrins in enteric neural crest cells leads to a Hirschsprung-like phenotype. *Development 133*, 1725-1734. https://doi.org/10.1242/dev.02346

Bremer, S. and Hartung, T. (2004). The use of embryonic stem cells for regulatory developmental toxicity testing in vitro – the current status of test development. *Curr Pharm Des 10*, 2733-2747. https://doi.org/10.2174/1381612043383700

Bronner-Fraser, M., Wolf, J. J. and Murray, B. A. (1992). Effects of antibodies against N-cadherin and N-CAM on the cranial neural crest and neural tube. *Dev Biol 153*, 291-301. https://doi.org/10.1016/0012-1606(92)90114-V

Crofton, K. M., Mundy, W. R., Lein, P. J. et al. (2011). Developmental neurotoxicity testing: Recommendations for developing alternative methods for the screening and prioritization of chemicals. *ALTEX 28*, 9-15. https://doi.org/10.14573/altex.2011.1.009

Crofton, K. M., Mundy, W. R. and Shafer, T. J. (2012). Developmental neurotoxicity testing: A path forward. *Congenit Anom (Kyoto) 52*, 140-146. https://doi.org/10.1111/j.1741-4520.2012.00377.x

de Araujo, W. M., Robbs, B. K., Bastos, L. G. et al. (2016). PTEN overexpression cooperates with lithium to reduce the malignancy and to increase cell death by apoptosis via PI3K/Akt suppression in colorectal cancer cells. *J Cell Biochem 117*, 458-469. https://doi.org/10.1002/jcb.25294

Dolk, H., Loane, M. and Garne, E. (2010). The prevalence of

congenital anomalies in Europe. *Rare Diseases Epidemiology 686*, 349-364. https://doi.org/10.1007/978-90-481-9485-8_20

Dreser, N., Zimmer, B., Dietz, C. et al. (2015). Grouping of histone deacetylase inhibitors and other toxicants disturbing neural crest migration by transcriptional profiling. *Neurotoxicology 50*, 56-70. https://doi.org/10.1016/j.neuro.2015.07.008

Farlie, P. G., McKeown, S. J. and Newgreen, D. F. (2004). The neural crest: Basic biology and clinical relationships in the craniofacial and enteric nervous systems. *Birth Defects Res C Embryo Today 72*, 173-189. https://doi.org/10.1002/bdrc.20013

Fritsche, E., Cline, J. E., Nguyen, N.-H. et al. (2005). Polychlorinated biphenyls disturb differentiation of normal human neural progenitor cells: Clue for involvement of thyroid hormone receptors. *Environ Health Perspect 113*, 871-876. https://doi.org/10.1289/ehp.7793

Fuller, L. C., Cornelius, S. K., Murphy, C. W. et al. (2002). Neural crest cell motility in valproic acid. *Reprod Toxicol 16*, 825-839. https://doi.org/10.1016/S0890-6238(02)00059-X

Grandjean, P. and Landrigan, P. J. (2014). Neurobehavioural effects of developmental toxicity. *Lancet Neurol 13*, 330-338. https://doi.org/10.1016/s1474-4422(13)70278-3

Green, S. A., Simoes-Costa, M. and Bronner, M. E. (2015). Evolution of vertebrates as viewed from the crest. *Nature 520*, 474-482. https://doi.org/10.1038/nature14436

Grimm, L. M., Goldberg, A. L., Poirier, G. G. et al. (1996). Proteasomes play an essential role in thymocyte apoptosis. *EMBO J 15*, 3835-3844.

Haack, H. and Hynes, R. O. (2001). Integrin receptors are required for cell survival and proliferation during development of the peripheral glial lineage. *Dev Biol 233*, 38-55. https://doi.org/10.1006/dbio.2001.0213

Hansson, O., Castilho, R. F., Kaminski Schierle, G. S. et al. (2000). Additive effects of caspase inhibitor and lazaroid on the survival of transplanted rat and human embryonic dopamine neurons. *Exp Neurol 164*, 102-111. https://doi.org/10.1006/exnr.2000.7406

Harrill, J. A., Robinette, B. L. and Mundy, W. R. (2011). Use of high content image analysis to detect chemical-induced changes in synaptogenesis in vitro. *Toxicol In Vitro 25*, 368-387. https://doi.org/10.1016/j.tiv.2010.10.011

Hartung, T. and Leist, M. (2008). Food for thought ... on the evolution of toxicology and the phasing out of animal testing. *ALTEX 25*, 91-102. http://www.altex.ch/en/All-issues/Issue.50.html?iid=99&aid=1

Hartung, T. (2009). Toxicology for the twenty-first century. *Nature 460*, 208-212. https://doi.org/10.1038/460208a

Heanue, T. A. and Pachnis, V. (2006). Expression profiling the developing mammalian enteric nervous system identifies marker and candidate Hirschsprung disease genes. *Proc Natl Acad Sci U S A 103*, 6919-6924. https://doi.org/10.1073/pnas.0602152103

Hoelting, L., Klima, S., Karreman, C. et al. (2016). Stem cell-derived immature human dorsal root ganglia neurons to identify peripheral neurotoxicants. *Stem Cells Transl Med 5*, 476-487. https://doi.org/10.5966/sctm.2015-0108

Huang, R., Xia, M., Sakamuru, S. et al. (2016). Modelling the Tox21 10 K chemical profiles for in vivo toxicity prediction and mechanism characterization. *Nat Commun 7*, 10425. https://doi.org/10.1038/ncomms10425

Inoue, T., Chisaka, O., Matsunami, H. et al. (1997). Cadherin-6 expression transiently delineates specific rhombomeres, other neural tube subdivisions, and neural crest subpopulations in mouse embryos. *Dev Biol 183*, 183-194. https://doi.org/10.1006/dbio.1996.8501

Kil, S. H., Krull, C. E., Cann, G. et al. (1998). The alpha4 subunit of integrin is important for neural crest cell migration. *Dev Biol 202*, 29-42. https://doi.org/10.1006/dbio.1998.8985

Kimura, Y., Matsunami, H., Inoue, T. et al. (1995). Cadherin-11 expressed in association with mesenchymal morphogenesis in the head, somite, and limb bud of early mouse embryos. *Dev Biol 169*, 347-358. https://doi.org/10.1006/dbio.1995.1149

Krug, A. K., Balmer, N. V., Matt, F. et al. (2013a). Evaluation of a human neurite growth assay as specific screen for developmental neurotoxicants. *Arch Toxicol 87*, 2215-2231. https://doi.org/10.1007/s00204-013-1072-y

Krug, A. K., Kolde, R., Gaspar, J. A. et al. (2013b). Human embryonic stem cell-derived test systems for developmental neurotoxicity: A transcriptomics approach. *Arch Toxicol 87*, 123-143. https://doi.org/10.1007/s00204-012-0967-3

Latta, M., Kunstle, G., Leist, M. et al. (2000). Metabolic depletion of ATP by fructose inversely controls CD95- and tumor necrosis factor receptor 1-mediated hepatic apoptosis. *J Exp Med 191*, 1975-1985. https://doi.org/10.1084/jem.191.11.1975

Lee, G., Chambers, S. M., Tomishima, M. J. et al. (2010). Derivation of neural crest cells from human pluripotent stem cells. *Nat Protoc 5*, 688-701. https://doi.org/10.1038/nprot.2010.35

Leist, M., Hartung, T. and Nicotera, P. (2008). The dawning of a new age of toxicology. *ALTEX 25*, 103-114. http://www.altex.ch/en/All-issues/Issue.50.html?iid=99&aid=3

Leist, M., Efremova, L. and Karreman, C. (2010). Food for thought ... considerations and guidelines for basic test method descriptions in toxicology. *ALTEX 27*, 309-317. https://doi.org/10.14573/altex.2010.4.309

Leist, M., Hasiwa, N., Rovida, C. et al. (2014). Consensus report on the future of animal-free systemic toxicity testing. *ALTEX 31*, 341-356. https://doi.org/10.14573/altex.1406091

Livak, K. J. and Schmittgen, T. D. (2001). Analysis of relative gene expression data using real-time quantitative PCR and the 2(-Delta Delta C(T)) Method. *Methods 25*, 402-408. https://doi.org/10.1006/meth.2001.1262

McKeown, S. J., Wallace, A. S. and Anderson, R. B. (2013). Expression and function of cell adhesion molecules during neural crest migration. *Dev Biol 373*, 244-257. https://doi.org/10.1016/j.ydbio.2012.10.028

Menegola, E., Broccia, M. L., Di Renzo, F. et al. (2005). Study on the common teratogenic pathway elicited by the fungicides triazole-derivatives. *Toxicol In Vitro 19*, 737-748. https://doi.org/10.1016/j.tiv.2005.04.005

Mica, Y., Lee, G., Chambers, S. M. et al. (2013). Modeling neural crest induction, melanocyte specification, and disease-related pigmentation defects in hESCs and patient-specific iPSCs. *Cell Rep 3*, 1140-1152. https://doi.org/10.1016/j.celrep.2013.03.025

Mould, A. P., Askari, J. A., Craig, S. E. et al. (1994). Integrin alpha 4 beta 1-mediated melanoma cell adhesion and migration on vascular cell adhesion molecule-1 (VCAM-1) and the alternatively spliced IIICS region of fibronectin. *J Biol Chem 269*, 27224-27230.

Nakagawa, S. and Takeichi, M. (1995). Neural crest cell-cell adhesion controlled by sequential and subpopulation-specific expression of novel cadherins. *Development 121*, 1321-1332.

Nakagawa, S. and Takeichi, M. (1998). Neural crest emigration from the neural tube depends on regulated cadherin expression. *Development 125*, 2963-2971.

Nicotera, P. and Leist, M. (1997). Mitochondrial signals and energy requirement in cell death. *Cell Death Differ 4*, 516. https://doi.org/10.1038/sj.cdd.4400275

Nieto, M. A. (2011). The ins and outs of the epithelial to mesenchymal transition in health and disease. *Annu Rev Cell Dev Biol 27*, 347-376. https://doi.org/10.1146/annurev-cellbio-092910-154036

Pennings, J. L., Theunissen, P. T. and Piersma, A. H. (2012). An optimized gene set for transcriptomics based neurodevelopmental toxicity prediction in the neural embryonic stem cell test. *Toxicology 300*, 158-167. https://doi.org/10.1016/j.tox.2012.06.016

Pla, P., Moore, R., Morali, O. G. et al. (2001). Cadherins in neural crest cell development and transformation. *J Cell Physiol 189*, 121-132. https://doi.org/10.1002/jcp.10008

Qiu, J. H., Asai, A., Chi, S. et al. (2000). Proteasome inhibitors induce cytochrome c-caspase-3-like protease-mediated apoptosis in cultured cortical neurons. *J Neurosci 20*, 259-265.

R Core Team (2015). *R: A Language and Environment for Statistical Computing*. Vienna, Austria: R Foundation for Statistical Computing. https://www.r-project.org/

Rempel, E., Hoelting, L., Waldmann, T. et al. (2015). A transcriptome-based classifier to identify developmental toxicants by stem cell testing: Design, validation and optimization for histone deacetylase inhibitors. *Arch Toxicol 89*, 1599-1618. https://doi.org/10.1007/s00204-015-1573-y

Ritz, C. and Streibig, J. C. (2005). Bioassay analysis using R. *J Stat Softw 12*, 1-22. https://doi.org/10.18637/jss.v012.i05

Rovida, C. and Hartung, T. (2009). Re-evaluation of animal numbers and costs for in vivo tests to accomplish REACH legislation requirements for chemicals – a report by the transatlantic think tank for toxicology t[4]. *ALTEX 26*, 187-208. https://doi.org/10.14573/altex.2009.3.187

Ryan, K. R., Sirenko, O., Parham, F. et al. (2016). Neurite outgrowth in human induced pluripotent stem cell-derived neurons as a high-throughput screen for developmental neurotoxicity or neurotoxicity. *Neurotoxicology 53*, 271-281. https://doi.org/10.1016/j.neuro.2016.02.003

Scholz, D., Poltl, D., Genewsky, A. et al. (2011). Rapid, complete and large-scale generation of post-mitotic neurons from the human LUHMES cell line. *J Neurochem 119*, 957-971. https://doi.org/10.1111/j.1471-4159.2011.07255.x

Selenica, M. L., Jensen, H. S., Larsen, A. K. et al. (2007). Efficacy of small-molecule glycogen synthase kinase-3 inhibitors in the postnatal rat model of tau hyperphosphorylation. *Br J Pharmacol 152*, 959-979. https://doi.org/10.1038/sj.bjp.0707471

Shellard, A. and Mayor, R. (2016). Chemotaxis during neural crest migration. *Semin Cell Dev Biol 55*, 111-118. https://doi.org/10.1016/j.semcdb.2016.01.031

Sheppard, A. M., Onken, M. D., Rosen, G. D. et al. (1994). Expanding roles for alpha 4 integrin and its ligands in development. *Cell Adhes Commun 2*, 27-43. https://doi.org/10.3109/15419069409014200

Shinde, V., Klima, S., Sureshkumar, P. S. et al. (2015). Human pluripotent stem cell based developmental toxicity assays for chemical safety screening and systems biology data generation. *J Vis Exp e52333*. https://doi.org/10.3791/52333

Sipes, N. S., Martin, M. T., Reif, D. M. et al. (2011). Predictive models of prenatal developmental toxicity from ToxCast high-throughput screening data. *Toxicol Sci 124*, 109-127. https://doi.org/10.1093/toxsci/kfr220

Smirnova, L., Hogberg, H. T., Leist, M. et al. (2014). Developmental neurotoxicity – challenges in the 21st century and in vitro opportunities. *ALTEX 31*, 129-156. https://doi.org/10.14573/altex.1403271

Stiegler, N. V., Krug, A. K., Matt, F. et al. (2011). Assessment of chemical-induced impairment of human neurite outgrowth by multiparametric live cell imaging in high-density cultures. *Toxicol Sci 121*, 73-87. https://doi.org/10.1093/toxsci/kfr034

Strobl-Mazzulla, P. H. and Bronner, M. E. (2012). Epithelial to mesenchymal transition: New and old insights from the classical neural crest model. *Semin Cancer Biol 22*, 411-416. https://doi.org/10.1016/j.semcancer.2012.04.008

Stummann, T. C., Hareng, L. and Bremer, S. (2009). Hazard assessment of methylmercury toxicity to neuronal induction in embryogenesis using human embryonic stem cells. *Toxicology 257*, 117-126. https://doi.org/10.1016/j.tox.2008.12.018

Taneyhill, L. A. (2008). To adhere or not to adhere: The role of Cadherins in neural crest development. *Cell Adh Migr 2*, 223-230. https://doi.org/10.4161/cam.2.4.6835

Testaz, S., Delannet, M. and Duband, J. (1999). Adhesion and migration of avian neural crest cells on fibronectin require the cooperating activities of multiple integrins of the (beta)1 and (beta)3 families. *J Cell Sci 112*, 4715-4728.

Testaz, S. and Duband, J. L. (2001). Central role of the alpha4beta1 integrin in the coordination of avian truncal neural crest cell adhesion, migration, and survival. *Dev Dyn 222*, 127-140. https://doi.org/10.1002/dvdy.1181

Theunissen, P. T., Robinson, J. F., Pennings, J. L. et al. (2012). Transcriptomic concentration-response evaluation of valproic acid, cyproconazole, and hexaconazole in the neural embryonic stem cell test (ESTn). *Toxicol Sci 125*, 430-438. https://doi.org/10.1093/toxsci/kfr293

Theunissen, P. T., Pennings, J. L., van Dartel, D. A. et al. (2013). Complementary detection of embryotoxic properties of substances in the neural and cardiac embryonic stem cell tests. *Toxicol Sci 132*, 118-130. https://doi.org/10.1093/toxsci/kfs333

Theveneau, E. and Mayor, R. (2012). Neural crest delamination and migration: From epithelium-to-mesenchyme transition to collective cell migration. *Dev Biol 366*, 34-54. https://doi.org/10.1016/j.ydbio.2011.12.041

Theveneau, E., Steventon, B., Scarpa, E. et al. (2013). Chase-and-run between adjacent cell populations promotes directional

collective migration. *Nat Cell Biol 15*, 763-772. https://doi.org/10.1038/ncb2772

Trainor, P. A. (2010). Craniofacial birth defects: The role of neural crest cells in the etiology and pathogenesis of Treacher Collins syndrome and the potential for prevention. *Am J Med Genet A 152A*, 2984-2994. https://doi.org/10.1002/ajmg.a.33454

Usami, M., Mitsunaga, K., Irie, T. et al. (2014). Simple in vitro migration assay for neural crest cells and the opposite effects of all-trans-retinoic acid on cephalic- and trunk-derived cells. *Congenit Anom (Kyoto) 54*, 184-188. https://doi.org/10.1111/cga.12059

Usami, M., Mitsunaga, K., Miyajima, A. et al. (2015). Effects of 13 developmentally toxic chemicals on the migration of rat cephalic neural crest cells in vitro. *Congenit Anom (Kyoto) 56*, 52-59. https://doi.org/10.1111/cga.12121

Vallin, J., Girault, J. M., Thiery, J. P. et al. (1998). Xenopus cadherin-11 is expressed in different populations of migrating neural crest cells. *Mech Dev 75*, 171-174. https://doi.org/10.1016/S0925-4773(98)00099-9

van Dartel, D. A., Pennings, J. L., Hendriksen, P. J. et al. (2009). Early gene expression changes during embryonic stem cell differentiation into cardiomyocytes and their modulation by monobutyl phthalate. *Reprod Toxicol 27*, 93-102. https://doi.org/10.1016/j.reprotox.2008.12.009

van Thriel, C., Westerink, R. H., Beste, C. et al. (2012). Translating neurobehavioural endpoints of developmental neurotoxicity tests into in vitro assays and readouts. *Neurotoxicology 33*, 911-924. https://doi.org/10.1016/j.neuro.2011.10.002

Vohra, B. P., Tsuji, K., Nagashimada, M. et al. (2006). Differential gene expression and functional analysis implicate novel mechanisms in enteric nervous system precursor migration and neuritogenesis. *Dev Biol 298*, 259-271. https://doi.org/10.1016/j.ydbio.2006.06.033

Volbracht, C., Leist, M. and Nicotera, P. (1999). ATP controls neuronal apoptosis triggered by microtubule breakdown or potassium deprivation. *Mol Med 5*, 477-489.

Waldmann, T., Rempel, E., Balmer, N. V. et al. (2014). Design principles of concentration-dependent transcriptome deviations in drug-exposed differentiating stem cells. *Chem Res Toxicol 27*, 408-420. https://doi.org/10.1021/tx400402j

Wang, Z., Zhang, X., Chen, S. et al. (2013). Lithium chloride inhibits vascular smooth muscle cell proliferation and migration and alleviates injury-induced neointimal hyperplasia via induction of PGC-1alpha. *PLoS One 8*, e55471. https://doi.org/10.1371/journal.pone.0055471

Weil, M., Jacobson, M. D., Coles, H. S. et al. (1996). Constitutive expression of the machinery for programmed cell death. *J Cell Biol 133*, 1053-1059. https://doi.org/10.1083/jcb.133.5.1053

Wu, C., Fields, A. J., Kapteijn, B. A. et al. (1995). The role of alpha 4 beta 1 integrin in cell motility and fibronectin matrix assembly. *J Cell Sci 108*, 821-829.

Yu, J., Vodyanik, M. A., Smuga-Otto, K. et al. (2007). Induced pluripotent stem cell lines derived from human somatic cells. *Science 318*, 1917-1920. https://doi.org/10.1126/science.1151526

Zimmer, B., Schildknecht, S., Kuegler, P. B. et al. (2011). Sensitivity of dopaminergic neuron differentiation from stem cells to chronic low-dose methylmercury exposure. *Toxicol Sci 121*, 357-367. https://doi.org/10.1093/toxsci/kfr054

Zimmer, B., Lee, G., Balmer, N. V. et al. (2012). Evaluation of developmental toxicants and signaling pathways in a functional test based on the migration of human neural crest cells. *Environ Health Perspect 120*, 1116-1122. https://doi.org/10.1289/ehp.1104489

Zimmer, B., Pallocca, G., Dreser, N. et al. (2014). Profiling of drugs and environmental chemicals for functional impairment of neural crest migration in a novel stem cell-based test battery. *Arch Toxicol 88*, 1109-1126. https://doi.org/10.1007/s00204-014-1231-9

Zurich, M. G., Honegger, P., Schilter, B. et al. (2000). Use of aggregating brain cell cultures to study developmental effects of organophosphorus insecticides. *Neurotoxicology 21*, 599-605.

Zurich, M. G., Eskes, C., Honegger, P. et al. (2002). Maturation-dependent neurotoxicity of lead acetate in vitro: Implication of glial reactions. *J Neurosci Res 70*, 108-116. https://doi.org/10.1002/jnr.10367

Conflict of interest

The authors declare no conflicts of interest.

Acknowledgements

This work was supported by the State of Baden Württemberg, the Doerenkamp-Zbinden Foundation, the DFG (RTG1331, KoRS-CB) and the European Project EU-ToxRisk. We are grateful to M. Kapitza, X. Dolde and the staff of the bioimaging center (BIC) and the flow cytometry facility (FlowKon) for invaluable experimental support.

Correspondence to

Marcel Leist, PhD
In vitro Toxicology and Biomedicine
Dept inaugurated by the Doerenkamp-Zbinden
Foundation at the University of Konstanz
University of Konstanz
Box 657
Universitaetsstr. 10
78457 Konstanz, Germany
Phone: +49 7531 88 5037
Fax: +49 7531 88 5039
e-mail: marcel.leist@uni-konstanz.de